

LEVERAGING DATA TO SAY NO: MEMORY AUGMENTED PLUG-AND-PLAY SELECTIVE PREDICTION

Aditya Sarkar^{1,2} Yi Li³ Jiacheng Cheng^{2,4,†} Shlok Mishra^{1,5} Nuno Vasconcelos²

¹University of Maryland, College Park ²University of California, San Diego

³Qualcomm AI ⁴Yale University ⁵Meta AI

ABSTRACT

Selective prediction aims to endow predictors with a reject option, to avoid low confidence predictions. However, existing literature has primarily focused on closed-set tasks, such as visual question answering with predefined options or fixed-category classification. This paper considers selective prediction for visual language foundation models, addressing a taxonomy of tasks ranging from closed to open set and from finite to unbounded vocabularies, as in image captioning. We seek training-free approaches of low-complexity, applicable to any foundation model and consider methods based on external vision-language model embeddings, like CLIP. This is denoted as *Plug-and-Play Selective Prediction* (PAPSP). We identify two key challenges: (1) *instability of the visual-language representations*, leading to high variance in image-text embeddings, and (2) *poor calibration of similarity scores*. To address these issues, we propose a *memory augmented* PAPSP (MA-PAPSP) model, which augments PAPSP with a retrieval dataset of image-text pairs. This is leveraged to reduce embedding variance by averaging retrieved nearest-neighbor pairs and is complemented by the use of contrastive normalization to improve score calibration. Through extensive experiments on multiple datasets, we show that MA-PAPSP outperforms PAPSP and other selective prediction baselines for selective captioning, image-text matching, and fine-grained classification. Code is publicly available at <https://github.com/kingston-aditya/MA-PaPSP>.

1 INTRODUCTION

The success of vision-language models (VLMs) enables a wide range of promising applications. However, these models are prone to erroneous predictions for reasons that include incorrect alignment of the two modalities, image or language ambiguities, or samples from the tails of their training distribution. This hampers their usefulness for real-world applications that require performance guarantees. As shown in Figure 1, *selective prediction* (SP) (Chow, 1957; 1970; El-Yaniv & Wiener, 2010; Whitehead et al., 2022; Dancette et al., 2023; Geifman & El-Yaniv, 2017; Wang & Vasconcelos, 2018; Srinivasan et al., 2024) methods address this problem by *refusing* to make low confidence predictions, with the goal of minimizing the prediction *risk* on the samples that they *accept*. Optimal selective predictors optimize the trade-off between *risk* and *coverage*, which is the acceptance ratio throughout a dataset. While there is a literature in SP, the problem has mostly been considered for *closed-set* prediction, usually with finite and small output vocabularies. Examples include classification with finite labels (Wang & Vasconcelos, 2018; Wu et al., 2020) or visual question answering from a finite set of choices (Wang et al., 2023; Dancette et al., 2023), *e.g.* binary questions, questions involving a finite set of attributes, etc. However, vision-language tasks like the *selective captioning* problem of Figure 1 require *open-set* prediction, where the label set is infinite. This is, in fact, the regime that most foundation models operate in. There is a need for SP methods for open set tasks.

One possibility is to endow the foundation model with some prediction refusal score and train or fine-tune it to optimize the ensuing risk-coverage trade-off. However, most foundation models are large and require large-scale training to avoid overfitting (Stevens et al., 2024; Gu et al., 2025). In many cases, the model may even be a proprietary black box that is impossible to retrain. In this

[†]Corresponding author: Jiacheng Cheng.

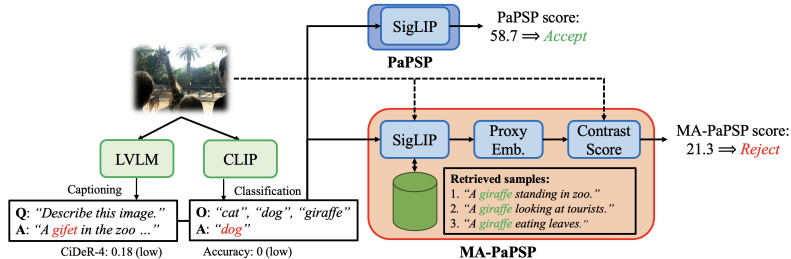


Figure 1: PAPSP uses an external representation model and the CLIP score to enable selective prediction for VLM tasks like captioning without training. MA-PAPSP augments this model with an external dataset, which is leveraged to estimate proxy embeddings of greater stability and better calibrated contrastive scores. The figure shows an example where PAPSP fails but MA-PAPSP succeeds at rejecting an incorrect caption for the image shown. Also shown is the Cider-4 score between predicted and ground truth captions.

work, we investigate an alternative solution, based on an *external SP model* that can be attached to any VLM, as illustrated in Figure 1, to compute a confidence score for the predictions of the latter. SP can then be implemented by rejecting predictions of score below a threshold. This is denoted as *Plug-and-Play Selective Prediction* (PAPSP) and can be implemented by using a Large Visual Language Model (LVLM), *e.g.* Qwen (Bai et al., 2023), InternVL (Zhu et al., 2025), as PAPSP model, in what is called the LLM-as-judge strategy (Dong et al., 2024; Ye et al., 2025). However, LVLMs are large and have computationally expensive inference, sometimes much heavier than the VLM which makes the original predictions. Furthermore, they are not calibrated for PAPSP and requires some type of training or adaptation, which can itself be expensive and induce overfitting. Ideally, the PAPSP model should be lightweight and flexible enough to support any task without training.

In this work, we investigate the use of a visual language representation models (VLRMs), like CLIP (Radford et al., 2021) or SigLIP (Zhai et al., 2023), to implement PAPSP. This is denoted as the *Selective Prediction-VLM* (SP-VLM). A simple yet effective implementation, illustrated in the top branch of Figure 1, is to project the image and text produced by the foundation model into the SP-VLM embedding and reject image-text pairs of low CLIP-score (Hessel et al., 2021). We find, however that SP-VLM embeddings also suffer from calibration shortcomings, which we hypothesize to have two main causes: 1) SP-VLM representation *instability*, which increases the variance of image and text embeddings, compromising the reliability of similarity scores, and 2) *poor calibration* of similarity score across the SP-VLM embedding. To overcome these, we propose the *Memory Augmented PAPSP* (MA-PAPSP) procedure of the lower branch of Figure 1. The external SP-VLM is augmented with a retrieval dataset of image-text pairs. Methods that leverage this dataset are then proposed to 1) reduce the variance of the SP-VLM representation, by using the average representation of the nearest neighbors of the query image as a *proxy embedding* for the latter, and 2) enhance score calibration, by using *contrastive scores* that normalize the similarity score with respect to alternative text predictions. MA-PAPSP can be seen as a new instantiation of *memory augmented* approaches recently shown successful for various applications (Nakata et al., 2022; Zeng et al., 2024; Geirhos et al., 2024; Silva et al., 2024). Like these, it is a *training-free* method that instead leverages an external dataset to enhance SP-VLM functionality.

MA-PAPSP has several interesting properties. First, it is a relatively lightweight solution, usually much lighter than an LVLM. Second, it requires no training of either foundation model or the SP-VLM. Third, it can implement SP over a taxonomy of foundation model tasks, including classification (Zhou et al., 2022a;b), image-text matching (Ma et al., 2023; Hsieh et al., 2024), and captioning, that range from closed to open set and from finite to unbounded prediction vocabularies. Fourth, it can be used with any foundation model. We show its effectiveness for models ranging from small VLRMs to large LVLMs. Finally, MA-PAPSP can be tailored to any application domain by simply collecting data from that domain. This usually leads to improved performance over PAPSP, as illustrated in Figure 1. We show this for domains ranging from COCO captioning to medical imaging and that good performance can be achieved even with generic datasets, like CC12M (Changpinyo et al., 2021), not directly tied to the application, for both open-set and closed-set SP tasks.

The contributions of this work are three-fold: 1) we formulate the PAPSP problem over a taxonomy of SP tasks, ranging from closed to open set and finite to unbounded vocabularies. To our knowledge, this is the first attempt to solve PAPSP for all these tasks; 2) we propose the lightweight, training free MA-PAPSP method, which leverages an external dataset to improve SP-VLM; and 3) we conduct an extensive evaluation demonstrating the efficacy of MA-PAPSP for selective captioning, image-text matching and classification tasks across a range of foundation models and application domains.

2 RELATED WORKS

Selective Prediction. The problem of learning to reject has been studied in machine learning for over fifty years, primarily for unimodal classification (Chow, 1957; 1970; Geifman & El-Yaniv, 2017; Wang & Vasconcelos, 2018; Black et al., 2022; Srinivasan et al., 2024). It aims to design models that abstain from making predictions of low confidence. Various metrics and frameworks have been proposed (Geifman & El-Yaniv, 2019; Wang & Vasconcelos, 2018; De Stefano et al., 2000). While these studies focus on selective classification and multi-way visual question-answering, where the label set is finite, MA-PAPSP targets the more challenging setting of open-set tasks (like selective captioning or image-text matching) where labels are sentences and their cardinality can be unbounded.

Image-Text Alignment Score. Selective prediction performance can be improved by model re-training (Dancette et al., 2023). However, for foundation models, this requires large scale training and is not practical for many applications. One possibility is to rely on external models, e.g. the LLM-as-judge strategy (Ye et al., 2025; Dong et al., 2024). However, these are memory and compute intensive. Recent studies have proposed using visual question-answering to assess image-text alignment, such as SeeTRUE (Yarom et al., 2023) or VQASquare Lin et al. (2024). However, even these approaches rely on complex models, with long inference times. We show that they underperform MA-PAPSP, which has lower complexity.

Retrieval-Augmented Scoring. Memory-augmented pipelines, first introduced for language generation (Lewis et al., 2020), have been extended to vision-language representation learning (Iscen et al., 2023a;b; Xie et al., 2023). While they do retrieval augmentation just like MA-PAPSP, most models’ pretraining is very similar to CLIPs, and as a result, they have the same limitations like CLIP *i.e.*unstable representations and uncalibrated scores. More related works are discussed in D.

3 PLUG AND PLAY SELECTIVE PREDICTION

A VLM $f : \mathcal{X} \times \mathcal{Y} \rightarrow \mathcal{Y}$ maps an image $\mathbf{x} \in \mathcal{X}$ and a text $\mathbf{t} \in \mathcal{Y}$ into a text sequence $\mathbf{y} \in \mathcal{Y}$. Modern VLMs support a wide range of tasks. In this work, we consider a taxonomy of tasks of increasing complexity, which we refer to as the *VLM task taxonomy* in the remainder of the paper.

Level 1 - Coarse-grained Discrimination: Tasks such as classification, where f predicts a finite label set $\mathcal{Y} = \{\mathbf{y}_k\}_{k=1}^C$.

Level 2 - Fine-grained Discrimination: Classification-style tasks where the labels in \mathcal{Y} are very similar. For example, in *image-text matching* (ITM), the model chooses between two similar image captions, *e.g.* “A girl walking a cat.” versus “A girl walking a dog.”

Level 3 - Language Production: Tasks like captioning, where \mathcal{Y} is unbounded, *e.g.* the set of sentences in English.

3.1 SELECTIVE PREDICTION

In many applications, there is value in identifying and abstaining from making prediction errors. *Selective prediction* (Chow, 1957; El-Yaniv & Wiener, 2010; Whitehead et al., 2022) implements this by augmenting the model output with an option to abstain \emptyset . A selective model $h : \mathcal{X} \rightarrow \mathcal{Y} \cup \{\emptyset\}$ usually composes the model $f : \mathcal{X} \rightarrow \mathcal{Y}$ with a selection function $g : \mathcal{X} \rightarrow \{0, 1\}$,

$$h(\mathbf{x}) = (f, g)(\mathbf{x}) = \begin{cases} f(\mathbf{x}) & \text{if } g(\mathbf{x}) = 1 \\ \emptyset & \text{if } g(\mathbf{x}) = 0. \end{cases}, \quad \text{where } g(\mathbf{x}) = \mathbb{1}[s(\mathbf{x}, f(\mathbf{x})) \geq \tau], \quad (1)$$

where $\mathbb{1}[\cdot]$ is the indicator function. If the selection function g decides that a prediction should be made, the model prediction f is output, otherwise h abstains. The selection function g is implemented by computing a score $s : \mathcal{X} \times \mathcal{Y} \rightarrow \mathbb{R}$ for the confidence of prediction $f(\mathbf{x})$ for image \mathbf{x} , which is compared to a confidence threshold $\tau \in \mathbb{R}$. Ideally, the score s should yield a high (low) value when $f(\mathbf{x})$ is correct (incorrect).

Selective prediction aims to optimize the trade-off between coverage and risk (El-Yaniv & Wiener, 2010). Given a set $\mathcal{D} = \{(\mathbf{x}_i, \mathbf{a}_i) \in \mathcal{X} \times \mathcal{Y}\}_{i=1}^{|\mathcal{D}|}$ of image \mathbf{x}_i and text \mathbf{a}_i (captions or class label) pairs, coverage is the proportion of examples for which a prediction is made

$$\mathcal{R}(f, g) = \frac{\frac{1}{|\mathcal{D}|} \sum_i \mathcal{L}(f(\mathbf{x}_i), \mathbf{a}_i) g(\mathbf{x}_i)}{\mathcal{C}(g)}, \quad \text{where } \mathcal{C}(g) = \frac{1}{|\mathcal{D}|} \sum_i g(\mathbf{x}_i), \quad (2)$$

while risk is the average loss on the covered subset, where $\mathcal{L} : \mathcal{Y} \times \mathcal{Y} \rightarrow \mathbb{R}$ is a loss function. In this work, we use the 0-1 loss function for classification problems and the loss

$$\mathcal{L}(f(\mathbf{x}_i), \mathbf{a}_i) = \begin{cases} 1 & \text{if } r(f(\mathbf{x}_i), \mathbf{a}_i) \geq \beta \\ 0 & \text{otherwise} \end{cases} \quad (3)$$

for captioning problems, where $r : \mathcal{Y} \times \mathcal{Y} \rightarrow \mathbb{R}$ is a measure of caption similarity, such as CiderN (Vedantam et al., 2015), or METEOR (Banerjee & Lavie, 2005) and $\beta \in \mathbb{R}$ a similarity threshold. We compute the Area Under the Risk-Coverage curve (AURC) (Geifman et al., 2019) for a summary of performance across different coverage levels. The lower the area, the better the model.

3.2 PLUG AND PLAY SELECTIVE PREDICTION (PAPSP)

Motivation. The tasks in the VLM task taxonomy can be performed by a multitude of models, including *visual language representation models* (VLRMs) like CLIP (Radford et al., 2021) or *large visual language models* (LVLMs) like LLaVA (Liu et al., 2023a). These are frequently large and/or black-box, in which cases selective prediction training is undesirable or impossible. To address this, we investigate the design of *plug-and-play selective prediction* (PAPSP) modules that can be attached to an existing VLM to implement the score function s of (1). Ideally, the PAPSP module should support an *open vocabulary*, be relatively light-weight, and require no training. However, selective prediction has mostly been studied for closed-set classification problems, where s can be derived from the posterior class probability estimates predicted by the classifier f . In fact, if the classifier produces calibrated probability estimates (Guo et al., 2017; Cheng & Vasconcelos, 2022), the largest class probability is the optimal score for the implementation of (1) (Chow, 1970).

For visual language tasks, the situation is far more complex. Because the normalization of probabilities by softmax type of operations is not feasible when \mathcal{Y} is unbounded, as in captioning, it is frequently impossible to obtain calibrated probability estimates for the model predictions. Unbounded prediction also introduces ambiguities, e.g. different captions can be semantically equivalent or otherwise match a given image, which do not appear in classification. To address this, we propose to implement PAPSP with an *external* CLIP-style VLRM, based on a pair of encoders of shared output space \mathcal{F}^e . An image $\mathbf{x} \in \mathcal{X}$ is mapped by an image encoder ϕ_{img}^e into a feature vector $\mathbf{v} = \phi_{\text{img}}^e(\mathbf{x}) \in \mathcal{F}^e$. Similarly, a caption $\mathbf{t} \in \mathcal{Y}$ is mapped by a text encoder ϕ_{txt}^e into a feature vector $\mathbf{w} = \phi_{\text{txt}}^e(\mathbf{t}) \in \mathcal{F}^e$. The encoder pair is pre-trained with a loss function that encourages the alignment of the feature vectors \mathbf{v} and \mathbf{w} in \mathcal{F}^e . Note the use of the e superscript to emphasize that the PAPSP model is *external*. The VLM making the original prediction f can also be a CLIP-style VLM, *e.g.* if the task is classification. To avoid confusion, we refer to the latter as the *predictive VLM* (P-VLM) and the VLM used to implement PAPSP as the *selective prediction VLM* (SP-VLM).

We hypothesize that, if the text ϕ_{txt}^e and image ϕ_{img}^e encoders of the SP-VLM differ from those of the P-VLM, an erroneous prediction $f(\mathbf{x})$ produced by latter is *unlikely* to induce a feature vector $\phi_{\text{txt}}^e(f(\mathbf{x}))$ close to the projection $\phi_{\text{img}}^e(\mathbf{x})$ of the image in the feature space \mathcal{F}^e of the SP-VLM. Hence, a natural implementation of (1) is to simply compute the similarity score in \mathcal{F}^e ,

$$s(\mathbf{x}, f(\mathbf{x})) = \cos(\phi_{\text{img}}^e(\mathbf{x}), \phi_{\text{txt}}^e(f(\mathbf{x}))). \quad (4)$$

This is known as the CLIP-score (Hessel et al., 2021). We denote its use in (1) as the PAPSP model and show that it has relatively weak selective prediction ability. We hypothesize that this is due

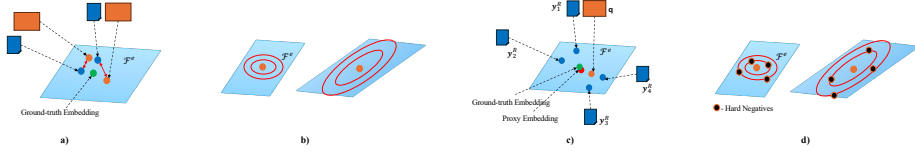


Figure 2: **Left:** VLM problems. a) *instability of representations*: the representations of images (orange) and texts (blue) of the same concept can vary significantly, leading to unreliable similarity scores. b) *poor calibration*: distances between concepts of identical similarity (red ellipses) vary across the VLM embedding \mathcal{F}^e . **Right:** PAPSP solutions: c) *proxy embeddings* of a query \mathbf{q} (orange) average multiple nearest neighbor representations from a retrieval dataset (blue) to produce a more stable representation (red), closer to the concept ground-truth (green). d) *contrastive scores* normalize similarity scores between image and predicted caption by those between the image and a set of hard-negatives, to ensure consistency across the space.

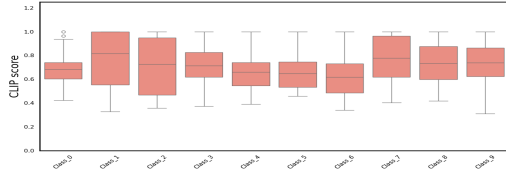


Figure 3: CLIP scores between class labels and images of the class.

Variant	Query	Proxy	Type
i2tr	$\phi_{\text{img}}(\mathbf{x})$	$\tilde{\phi}_{\text{txt}}^e(\mathbf{x})$	cross-modal
i2ir	$\phi_{\text{img}}(\mathbf{x})$	$\tilde{\phi}_{\text{img}}^e(\mathbf{x})$	uni-modal
t2tr	$\phi_{\text{txt}}(f(\mathbf{x}))$	$\tilde{\phi}_{\text{txt}}^e(f(\mathbf{x}))$	uni-modal
t2ir	$\phi_{\text{txt}}(f(\mathbf{x}))$	$\tilde{\phi}_{\text{img}}^e(f(\mathbf{x}))$	cross-modal

Table 1: Variants of retrieval-based proxy embeddings supported by MA-PAPSP.

to two problems. The first is that the SP-VLM feature space is somewhat *unstable*, producing an imperfect alignment of images and text. This can be due to either poor training or just the ambiguity of image-text alignment, since different sentences can have similar meaning and sentences with almost the same words can have very different meaning. In result, as illustrated in Figure 2 a), there can be non-trivial variability across images (orange) and texts (blue) of the same groundtruth concept and the similarity scores of two equivalent image-text pairs can be quite different. The second is that while scores computed in \mathcal{F}^e are effective for relative judgments of similarity, such softmax classification, they are too *poorly calibrated* for the absolute judgments required by the selection function g . As illustrated in Figure 2 b), the distances between an image or a text and semantically equivalent examples can vary significantly depending on the location of \mathcal{F}^e where they are projected.

We tested these hypotheses on UCF-101 (Soomro et al., 2012). Class labels and images per class were projected into the feature space \mathcal{F}^e of CLIP_{B/16}. The score of (4) was then computed between images and their labels. Figure 3 shows that certain classes have high score variance, confirming the instability of the semantic representation. Some classes also exhibit much higher variance than others, confirming that the representation is poorly calibrated for certain classes or regions of \mathcal{F}^e . While these problems can be ameliorated by fine-tuning the SP-VLM on the target data, this can overfit and degrade model generalization. Fine-tuning is challenging for open set problems, like captioning, where the boundaries of “application data” are not even well defined.

4 MEMORY AUGMENTED PAPSP (MA-PAPSP)

To improve the performance of PAPSP without training, we propose to complement the pre-trained SP-VLM with retrieval augmentation, as illustrated in Figure 4. This is denoted as *Memory Augmented PAPSP* (MA-PAPSP) and relies on a reference dataset $\mathcal{R} = \{(\mathbf{x}_i^R, \mathbf{y}_i^R)\}_{i=1}^{|\mathcal{R}|}$ of image-text pairs. The corresponding image-text projections $\{\mathbf{z}_i^R = (\phi_{\text{img}}^e(\mathbf{x}_i^R), \phi_{\text{txt}}^e(\mathbf{y}_i^R))\}_{i=1}^{|\mathcal{R}|}$ in \mathcal{F}^e are leveraged to address the instability and calibration problems of the pre-trained \mathcal{F}^e using the two blocks of the figure, which are discussed next.

Proxy Embeddings. To overcome the instability of the pre-trained \mathcal{F}^e , MA-PAPSP estimates the groundtruth embedding of a query \mathbf{q} by a *proxy embedding* $\tilde{\phi}_{\text{mod}}^e(\mathbf{q})$. The query \mathbf{q} can be an image \mathbf{x} or a text \mathbf{y} and **mod** the image or text modality. The proxy embedding is computed in two steps.

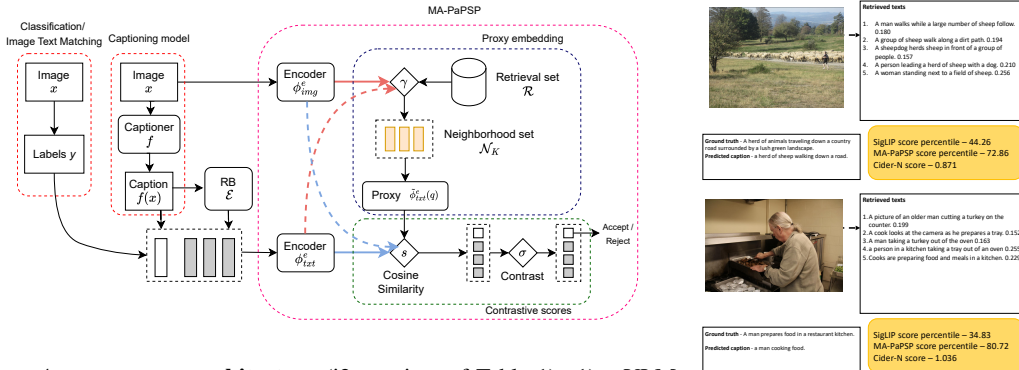


Figure 4: **MA-PAPSP architecture** (i2tr variant of Table 1). 1) a VLM encoder extracts a query image embedding $\phi_{img}^e(\mathbf{x})$. 2) This is used to retrieve a set \mathcal{N}_k of image-caption pairs from retrieval set \mathcal{R} . 3) The captions in this set are used to compute a proxy embedding $\tilde{\phi}_{txt}^e(f(\mathbf{x}))$, which is a weighted average of the retrieved text embeddings according to (6). This serves as an estimate of the ground-truth caption of $\phi_{img}^e(\mathbf{x})$. 4) A text embedding $\phi_{txt}^e(\mathbf{x})$ is computed for the caption predicted by (in image captioning) or chosen by (in image-text matching) the VLM. 5) The MA-PAPSP score is computed by computing the cosine similarity between predicted, $\phi_{img}^e(\mathbf{x})$, and estimated groundtruth, $\tilde{\phi}_{txt}^e(f(\mathbf{x}))$, captions and using (8) to compute a contrastive score. For image captioning, this leverages a set of hard-negative captions produced by an RB approach.

First, the K nearest neighbors of \mathbf{q} are retrieved from \mathcal{R} to form a neighborhood set

$$\mathcal{N}_K(\mathbf{q}) = \{(\mathbf{x}_i^R, \mathbf{y}_i^R) \in \mathcal{R} | i \in \mathcal{I}_K(\mathbf{q})\} \quad (5)$$

where $\mathcal{I}_K(\mathbf{q})$ is the set of indexes of K nearest neighbors of \mathbf{q} in \mathcal{R} . Retrieval is based on a similarity measure $\gamma(\mathbf{q}, \mathbf{z}_i^R)$, which can be either a measure of uni-modal similarity between images or between text vectors or a measure of cross-modal similarity between image and text vectors. The proxy embedding is then computed by averaging neighbors according to their proximity to \mathbf{q}

$$\tilde{\phi}_{mod}^e(\mathbf{q}) = \sum_{i \in \mathcal{I}_K(\mathbf{q})} \frac{\gamma(\mathbf{q}, \mathbf{z}_i^R)}{\sum_{j \in \mathcal{I}_K(\mathbf{q})} \gamma(\mathbf{q}, \mathbf{z}_j^R)} \phi_{mod}^e(\mathbf{y}_i^R). \quad (6)$$

Note that these operations can produce a text proxy $\tilde{\phi}_{txt}^e(\mathbf{q})$ or an image proxy $\tilde{\phi}_{img}^e(\mathbf{q})$ for \mathbf{q} , independently of whether \mathbf{q} is an image or a text. Table 1 summarizes the possible variants. Proxies of the modality of the query are denoted uni-modal, otherwise they are cross-modal.

Figure 2 (c) illustrates the computation of the proxy embedding $\tilde{\phi}_{txt}^e(\mathbf{q})$, where \mathbf{q} is an image and γ a cross-modal similarity function that retrieves the neighborhood set $\mathcal{N}_4(\mathbf{q})$ of 4 neighboring texts, which are used in the averaging operation of (6). This reduces the instability of the projections of the text embeddings in \mathcal{F}^e and produces a proxy embedding closer to the ground-truth concept than any of the retrieved texts, thereby reducing the instability problem of Figure 2 (a). Figure 5 shows some real examples, where \mathbf{q} is an image and 5 captions are retrieved from \mathcal{R} per example.

Contrastive Scores. Given the greater stability of the proxy representations, the simple replacement of the PAPSP similarity score of (4) by a score based on either the image-based proxy $\tilde{\phi}_{img}^e(\mathbf{x})$

$$s^{ip}(\mathbf{x}, f(\mathbf{x})) = \cos(\tilde{\phi}_{img}^e(\mathbf{x}), \phi_{txt}^e(f(\mathbf{x}))) \quad \text{or} \quad s^{tp}(\mathbf{x}, f(\mathbf{x})) = \cos(\tilde{\phi}_{txt}^e(\mathbf{x}), \phi_{txt}^e(f(\mathbf{x}))) \quad (7)$$

or the text-based proxy $\tilde{\phi}_{txt}^e(\mathbf{x})$ should improve the selective prediction performance of the SP-VLM. This, however, does not address the poor calibration of the pretrained \mathcal{F}^e , illustrated in Figure 2 (b). The problem is that due to local variations of the geometry of this space, the cosine similarities between a feature vector (orange dot) and its neighbors of fixed semantic similarity (red ellipses) vary depending on the \mathcal{F}^e location. To overcome this, we propose a to implement MA-PAPSP with

a text-based contrastive score

$$s^{\text{tc}}(\mathbf{x}, f(\mathbf{x}), \mathcal{E}(f(\mathbf{x}))) = \frac{\exp(s^{\text{tp}}(\mathbf{x}, f(\mathbf{x}))/\tau)}{\sum_{\mathbf{y}_k \in \mathcal{E}(f(\mathbf{x}))} \exp(s^{\text{tp}}(\mathbf{x}, \mathbf{y}_k)/\tau)} \quad (8)$$

where $\mathcal{E}(f(\mathbf{x}))$ is a set of hard-negative captions produced from the P-VLM prediction $f(\mathbf{x})$. In our implementation, these are obtained by replacing the nouns in $f(\mathbf{x})$ with a different set of nouns, which significantly alter caption meaning. For this, we either used a small language model (SLM) or a rule based approach (RB) to ensure constructing a meaningful sentence that is very different from the main caption. This operation produces a set of close neighbors of $f(\mathbf{x})$ with varying degrees of semantic similarity. The normalization of (8) by the scores of these neighbors results in two scores in $[0, 1]$, which have much more uniform magnitudes across the SP-VLM embedding \mathcal{F}^e than the non-contrastive scores of (7), as illustrated in Figure 2 (d). This is similar to the stronger homogeneity of softmax outputs than input logits for any classifier. Rule-based approach is discussed in supplementary section C, and the SLM prompt used in our experiments for generating negatives is discussed in E. Note that hard-negatives are not needed for the classification and ITM tasks, since these already define a set of alternative labels.

Figure 4 summarizes the proposed MA-PAPSP architecture. Given image \mathbf{x} , a P-VLM produces caption $f(\mathbf{x})$. The MA-PAPSP selective prediction model starts by mapping these into a pair of feature vectors, $\phi_{\text{img}}^e(\mathbf{x})$ and text $\phi_{\text{txt}}^e(f(\mathbf{x}))$, using the encoder pair of the SP-VLM. Either the image or text-based feature vector can then be used as a query \mathbf{q} . This is used to retrieve a set of K image text-image pairs from a retrieval dataset \mathcal{R} , which are used to generate a proxy embedding for \mathbf{q} with (6). This can be an embedding $\tilde{\phi}_{\text{txt}}^e(\mathbf{q})$ based on the retrieved texts, or an embedding $\tilde{\phi}_{\text{img}}^e(\mathbf{q})$ based on the retrieved images. The proxy embeddings are then used to compare a similarity score between image \mathbf{x} and caption $f(\mathbf{x})$. This can be implemented with the *base scores* of (7) or the *contrastive score* of (8), which rely on a set \mathcal{E} of hard negative variants of the caption $f(\mathbf{x})$ produced by RB, for captioning, or a set of class labels $\{\phi_{\text{txt}}(\mathbf{w}_k)\}_{k=1}^{|\mathcal{V}|}$, for classification.

5 EXPERIMENTS

In this section, we report on selective prediction experiments for three tasks representative of the different levels of the VLM task taxonomy: classification, image matching, and captioning.

Retrieval Set. We considered three types of retrieval sets: 1) **in-domain** retrieval set of training samples of the evaluation dataset, *e.g.* training split of MS-COCO (110K); 2) **out-of-domain** retrieval set combining Conceptual Caption CC12M and CC3M (Changpinyo et al., 2021) and SBU-1M (Ordonez et al., 2011), which have no overlap with any of the evaluation datasets, captioned using BLIP-2; 3) a **mixed** dataset concatenating the two above. In all cases, there is *no overlap* between evaluation and retrieval sets. **Out-of-domain** was used for retrieval unless otherwise specified.

Predictive-VLM. For classification and ITM, we compared P-VLMs of different different sizes (base and large). We present results for SigLIP (Zhai et al., 2023) in the paper and for other models in supplementary section C. For captioning, we mostly used BLIP w/ ViT-B (Li et al., 2022), but also present results for InternVL (Zhu et al., 2025) and Qwen-2.5-VL (Bai et al., 2023). RB approach used in our experiments is described in C.

Selective Prediction-VLM. We compare various SP-VLMs of different sizes and present results for SigLIP (Zhai et al., 2023) in the paper and other models in supplementary section C. PAPSP (X) denotes the implementation of PAPSP with SP-VLM X. X is omitted for the default SigLIP_{SO-400M}.

Metrics. Performance is evaluated with the risk and coverage measures of section 3. For captioning, the threshold β of (3) was set to 0.6 and 0.24 for Cider-N (N = 4 for all the experiments) and METEOR respectively. These thresholds were obtained empirically. Fig. 5 shows examples of captions that are above/below these thresholds for different metrics.

Baselines. PAPSP is compared to two Image-Text Alignment (ITA) scoring methods: VQASquare (Lin et al., 2024) and SeeTRUE (Yarom et al., 2023). More comparisons can be found in supplementary section B.

Results. We performed many experiments to evaluate the effectiveness of MA-PAPSP. Due to space limitations, we present most of the ablations (size of the neighborhood set \mathcal{N}_K and retrieval

Methods	Captioning				Classification			ITM				
	MS-COCO		Flickr-30K		Flowers	Pets	UCF101	SugarCrepe	Winoground	What'sUp	VL-Checklist	Foil
	Cider-N	Meteor	Cider-N	Meteor								
VQAScore	0.146	0.321	0.241	0.312	0.211	0.207	0.217	0.146	0.240	0.236	0.226	0.217
SeeTRUE	0.158	0.316	0.251	0.411	0.214	0.213	0.171	0.153	0.242	0.236	0.234	0.223
PAPSP-S	0.142	0.317	0.237	0.311	0.093	0.211	0.154	0.162	0.258	0.262	0.258	0.245
MA-PAPSP-S	0.121	0.312	0.235	0.310	0.077	0.171	0.116	0.079	0.228	0.214	0.210	0.213
Gain (S)	14.78	1.57	0.84	3.25	17.20	18.95	24.67	51.23	3.00	18.32	18.60	13.06
PAPSP-L	0.136	0.311	0.229	0.307	0.074	0.169	0.113	0.078	0.208	0.202	0.204	0.197
MA-PAPSP-L	0.109	0.286	0.219	0.297	0.063	0.114	0.088	0.062	0.196	0.192	0.192	0.189
Gain (L)	19.85	8.03	4.36	3.25	14.86	32.52	22.12	20.51	5.76	4.90	5.88	4.06

Table 2: Selective prediction AURC (\downarrow). S denotes the use of a small SP-VLM ($\text{SigLIP}_{B/16}$), while L denotes the larger $\text{SigLIP}_{SO-400M}$. ‘Gain’ is the % improvement of MA-PAPSP over PAPSP. ‘Gain (B)’ shows the same for $\text{SigLIP}_{B/16}$.

Retrieval Set	Captioning				Classification			ITM				
	MS-COCO		Flickr-30K		Flowers	Pets	UCF-101	SugarCrepe	Winoground	What'sUp	VL-checklist	Foil
	Cider-N	Meteor	Cider-N	Meteor								
Random	0.126	0.288	0.234	0.325	0.062	0.228	0.232	0.064	0.321	0.349	0.307	0.311
In-Domain	0.126	0.288	0.229	0.307	0.062	0.076	0.078	0.066	0.192	0.189	0.207	0.167
Out-of-Domain	0.109	0.286	0.219	0.297	0.063	0.114	0.088	0.062	0.196	0.192	0.192	0.189
Mixed	0.107	0.282	0.219	0.296	0.062	0.078	0.084	0.068	0.192	0.179	0.177	0.154

Table 3: Impact of retrieval set type on the AURC (\downarrow) of MA-PAPSP for captioning, classification, and ITM. Random dataset: MS-COCO for captioning, Flowers for classification, and SugarCrepe for ITM. **Blue** denotes improved performance of out-of-domain vs in-domain and **boldface** the best results.

set \mathcal{R} , proxy embedding variants of Table 1, inference latency, design choices, PAPSP with finetuned CLIP) on the supplemental sections B and C. In this section, we ablate the components of the MA-PAPSP architecture and present comparisons to competing techniques. MA-PAPSP is implemented with the image-to-text retrieval (i2tr) variant of Table 1 and the contrastive score of (8).

Selective captioning, ITM, and Classification. Table 2 summarizes performance for tasks in the three levels of the VLM task taxonomy. Several conclusions can be drawn. First, the VQAScore and SeeTRUE baselines underperformed even the implementation of MA-PAPSP with the smallest SP-VLM we tried (MA-PAPSP-S). This happens despite the fact that VQAScore and SeeTRUE rely on multiple LLM inferences to produce the selective prediction score and are thus much more computationally expensive. These results demonstrate the effectiveness of MA-PAPSP. Second, MA-PAPSP significantly outperforms PAPSP for equal SP-VLM (% gains shown in green). For example, with small SP-VLM, on 7 of the 10 datasets at least one metric improves by $\approx 15\%$ or more. In fact, MA-PAPSP using a small SP-VLM ($\text{SigLIP}_{B/16}$ - 16M parameters) outperforms PAPSP with a much larger SP-VLM ($\text{SigLIP}_{SO-400M}$ - 1B parameters) on all captioning and classification tasks. Third, both PAPSP and MA-PAPSP benefit from larger SP-VLMs, which usually have a more stable representation. Note that the gains of MA-PAPSP over PAPSP are *larger* for the larger model (L) on most captioning and classification tasks. This suggests that representation instability and, consequently, the effectiveness of MA-PAPSP hold independently of the model size. Fourth, the overall gains of the best version of MA-PAPSP (L) over the best LVL baseline (VQAScore) are very significant in all tasks. Finally, comparing the performance differences across tasks, it can be seen that MA-PAPSP has the largest gains for classification and captioning. For ITM, the gains over PAPSP are large on SugarCrepe but less pronounced on the remaining datasets.

Impact of the Retrieval Dataset. Table 3 shows how the type of retrieval dataset impacts MA-PAPSP performance. Beyond the in-domain, out-of-domain and mixed datasets, we also present results for a random dataset, which is one of the task datasets. Comparing the random with in-domain results shows that the training dataset of a domain (e.g. Flowers classification) has good performance for that domain (e.g. Flowers classification) but weaker performance for the remaining domains (e.g. Pets classification). Comparing the in-domain and out-of-domain results, it can be seen that the out-of-domain dataset overcomes this problem. For captioning, out-of-domain retrieval outperforms in-domain for all datasets. For ITM, which combines language and fine-grained

P-VLM	Model	MS-COCO		Flickr-30K	
		Cider-N	Meteor	Cider-N	Meteor
BLIP-1 (0.1B)	PAPSP	0.138	0.320	0.233	0.313
	MA-PAPSP	0.114	0.286	0.211	0.289
BLIP-2 (2.7B)	PAPSP	0.136	0.311	0.229	0.307
	MA-PAPSP	0.109	0.286	0.219	0.297
InternVL-3.5 (4B)	PAPSP	0.106	0.206	0.119	0.207
	MA-PAPSP	0.068	0.152	0.089	0.165
Qwen-2.5-VL (7B)	PAPSP	0.102	0.204	0.106	0.168
	MA-PAPSP	0.066	0.162	0.092	0.151

Table 4: Selective captioning AURC (↓) for different P-VLMs. In all cases, the SP-VLM is $\text{SigLIP}_{\text{SO400M}/14}$.

RS	SP-VLM	CheXpert		MIMIC-CXR	
		Cider-N	Meteor	Cider-N	Meteor
PAPSP					
		$\text{SigLIP}_{\text{SO400M}}$	0.264	0.313	0.272
		BioMedCLIP	0.164	0.238	0.175
MA-PAPSP					
Out-of-domain	$\text{SigLIP}_{\text{SO400M}}$	0.252	0.326	0.275	0.276
CheXpert	$\text{SigLIP}_{\text{SO400M}}$	0.137	0.276	0.157	0.326
MIMIC-CXR	$\text{SigLIP}_{\text{SO400M}}$	0.134	0.215	0.143	0.292
Mixed	$\text{SigLIP}_{\text{SO400M}}$	0.136	0.217	0.132	0.272
CheXpert	BioMedCLIP	0.126	0.198	0.142	0.216
MIMIC-CXR	BioMedCLIP	0.138	0.208	0.124	0.202
Mixed	BioMedCLIP	0.136	0.204	0.138	0.268

Table 5: AURC (↓) for biomedical models and datasets.

discrimination, the two dataset categories have similar results. This shows that relying on a larger *generic* (out-of-domain) dataset (15M samples) can outperform or achieve similar performance to a smaller in-domain dataset (*e.g.* 110K MS-COCO samples), for most language tasks. It is only for classification, a very fine-grained task that requires almost no language modeling, that the in-domain dataset is usually superior. However, the out-of-domain dataset is vastly superior to a small domain specific dataset mismatched to the target domain (see random for Pets and UCF-101). Finally, the mixed dataset achieves the best of both worlds, obtaining the best results for almost all tasks and datasets. Overall, it can be inferred that MA-PAPSP performance depends on both *size* and *domain coverage* of the retrieval set. A large generic dataset performs quite well, but can be outperformed by smaller retrieval sets covering the target domain, especially for classification. If the retrieval set is small and does not cover the target domain, performance degrades. We note that the choice of retrieval set is more of a problem for open-set problems like captioning and ITM. For classification, we found that a *small number* of samples (15) suffices.

Generalization across P-VLMs. Table 4 compares the selective captioning performance of PAPSP and MA-PAPSP for various P-VLMs, including BLIP and two LVLM models. Two conclusions can be inferred. First, for both methods, performance improves with P-VLM model size. This is because the captions generated by larger models LLMs are closer to ground truth captions. Second, while MA-PAPSP outperforms PAPSP irrespective of P-VLM size, the gains increase for the larger P-VLMs. This suggests that MA-PAPSP should be effective for even larger models.

Generalization to Specialized Domains. To test the flexibility of MA-PAPSP, we considered the worst-case scenario of applying it to very specialized domains for which neither the P-VLM or the SP-VLM are specifically trained. These experiments addressed selective captioning on the medical datasets CheXpert-5x200 (Irvin et al., 2019) and MIMIC-CXR-5x200 (Johnson et al., 2019), using Qwen-2.5-VL (7B) as P-VLM. We compared generic versions of PAPSP and MA-PAPSP ($\text{SigLIP}_{\text{SO-400M}}$ and the out-of-domain dataset) to implementations of PAPSP and MA-PAPSP with a specialized SP-VLM, BioMedCLIP (Zhang et al., 2023), and three retrieval sets: CheXpert, MIMIC-CXR, and a mixed dataset combining the above plus ROCO (Rückert et al., 2024), PadChart (de Castro et al., 2025), COVID (Shuja et al., 2020) and RSNA (Colak et al., 2021). Ground truth captions were created with template: “*An image of {class label}*”. The results of table 5 support the following conclusions. First, for comparable SP-VLM, PAPSP was comparable to MA-PAPSP with the out-of-domain dataset but much weaker than MA-PAPSP with any of the specialized datasets. In fact, starting from generic PAPSP ($\text{SigLIP}_{\text{SO-400M}}$), it is more beneficial to maintain the SP-VLM and use MA-PAPSP with specialized datasets than to implement PAPSP with the specialized SP-VLM (BioMedCLIP). This confirms the power and flexibility of MA-PAPSP. Second, with the specialized SP-VLM (BioMedCLIP) all specialized retrieval sets achieved results similar to the best obtained on domains like MS-COCO. This illustrates how MA-PAPSP can leverage models and data that are available already to cover a vast spectrum of domains without training.

Proxy estimation and Contrastive components. Table 6 presents an ablation study of the two main components of MA-PAPSP. Starting from the PAPSP model, both proxy estimation and con-

Proxy	Contrastive	Captioning		Classification			ITM				
		MS-COCO	Flickr-30K	Flowers	UCF-101	Pets	SugarCrepe	WinoGround	What'sUp	VL-Check	Foil
✗	✗	0.160	0.243	0.172	0.143	0.178	0.204	0.237	0.231	0.232	0.242
✓	✗	0.143	0.239	0.152	0.147	0.163	0.174	0.223	0.231	0.222	0.216
✗	✓	0.156	0.241	0.121	0.142	0.136	0.082	0.199	0.202	0.206	0.198
✓	✓	0.109	0.219	0.063	0.114	0.088	0.062	0.196	0.192	0.192	0.189

Table 6: AURC (\downarrow) ablation of the impact of proxy embedding and contrastive scores on MA-PAPSP. In all cases, the SP-VLM is SigLIP_{SO-400M}.

trastive scores improve AURC performance and the combination of the two provides an additional gain. This is evidence in support of the two hypothesis of Figure 2, namely the high variance of the SP-VLM representation and its poor calibration. The gains are larger for classification, followed by ITM, and captioning, suggesting greater benefits for finer-grained tasks.

6 LIMITATIONS AND CONCLUSION

This work extends the problem of selective prediction for foundation models to open-set problems such as captioning. We proposed MA-PAPSP, a memory-augmented approach that leverages an external visual language representation model and a dataset of text-image pairs to improve embedding stability and calibration of similarity scores. This enables a lightweight solution, that requires no training and can be applied to any foundation model. Experiments on a taxonomy of visual-language tasks demonstrated the effectiveness, flexibility, and robustness of MA-PAPSP for a range of foundation models. However, they have also shown that performance depends on the overlap between the retrieval set and the target application domain. While large generic datasets can achieve good performance, specialized datasets and even representation models may enable non-trivial gains for specialized domain, as we have demonstrated for medical imaging. This may require some trial and error by practitioners, to achieve the very best performance on a specific domain.

ACKNOWLEDGMENT

This work was partially funded by NSF awards IIS-2303153 and NAIRR-240300, the NVIDIA Academic grant, and a gift from Qualcomm. We also acknowledge the NRP Nautilus cluster, used for some of the experiments discussed above.

REFERENCES

Jinze Bai, Shuai Bai, Yunfei Chu, Zeyu Cui, Kai Dang, Xiaodong Deng, Yang Fan, Wenbin Ge, Yu Han, Fei Huang, et al. Qwen technical report. *arXiv preprint arXiv:2309.16609*, 2023.

Satanjeev Banerjee and Alon Lavie. Meteor: An automatic metric for mt evaluation with improved correlation with human judgments. In *Proceedings of the acl workshop on intrinsic and extrinsic evaluation measures for machine translation and/or summarization*, pp. 65–72, 2005.

Emily Black, Klas Leino, and Matt Fredrikson. Selective ensembles for consistent predictions. In *ICLR*, 2022.

Soravit Changpinyo, Piyush Sharma, Nan Ding, and Radu Soricut. Conceptual 12m: Pushing web-scale image-text pre-training to recognize long-tail visual concepts. In *CVPR*, 2021.

Jiacheng Cheng and Nuno Vasconcelos. Calibrating deep neural networks by pairwise constraints. In *CVPR*, 2022.

C. Chow. On optimum recognition error and reject tradeoff. *IEEE Transactions on information theory (TIT)*, 16(1):41–46, 1970.

Chi-Keung Chow. An optimum character recognition system using decision functions. *IRE Transactions on Electronic Computers*, 4:247–254, 1957.

Errol Colak, Felipe C Kitamura, Stephen B Hobbs, Carol C Wu, Matthew P Lungren, Luciano M Prevedello, Jayashree Kalpathy-Cramer, Robyn L Ball, George Shih, Anouk Stein, et al. The rsna pulmonary embolism ct dataset. *Radiology: Artificial Intelligence*, 3(2):e200254, 2021.

Corentin Dancette, Spencer Whitehead, Rishabh Maheshwary, Ramakrishna Vedantam, Stefan Scherer, Xinlei Chen, Matthieu Cord, and Marcus Rohrbach. Improving selective visual question answering by learning from your peers. In *CVPR*, 2023.

Daniel Coelho de Castro, Aurelia Bustos, Shruthi Bannur, Stephanie L Hyland, Kenza Bouzid, Maria Teodora Wetscherek, Maria Dolores Sánchez-Valverde, Lara Jaques-Pérez, Lourdes Pérez-Rodríguez, Kenji Takeda, et al. Padchest-gr: A bilingual chest x-ray dataset for grounded radiology report generation. *NEJM AI*, 2(7):AIdbp2401120, 2025.

Claudio De Stefano, Carlo Sansone, and Mario Vento. To reject or not to reject: that is the question—an answer in case of neural classifiers. *IEEE Transactions on Systems, Man, and Cybernetics, Part C (Applications and Reviews)*, 30(1):84–94, 2000.

Xinpeng Ding, Nannan Wang, Shiwei Zhang, De Cheng, Xiaomeng Li, Ziyuan Huang, Mingqian Tang, and Xinbo Gao. Support-set based cross-supervision for video grounding. In *Proceedings of the IEEE/CVF International Conference on Computer Vision*, pp. 11573–11582, 2021.

Yijiang River Dong, Tiancheng Hu, and Nigel Collier. Can llm be a personalized judge? *arXiv preprint arXiv:2406.11657*, 2024.

Matthijs Douze, Alexandr Guzhva, Chengqi Deng, Jeff Johnson, Gergely Szilvassy, Pierre-Emmanuel Mazaré, Maria Lomeli, Lucas Hosseini, and Hervé Jégou. The faiss library. *arXiv preprint arXiv:2401.08281*, 2024.

Ran El-Yaniv and Yair Wiener. On the foundations of noise-free selective classification. *Journal of Machine Learning Research (JMLR)*, 11(53):1605–1641, 2010.

Yuxin Fang, Quan Sun, Xinggang Wang, Tiejun Huang, Xinlong Wang, and Yue Cao. Eva-02: A visual representation for neon genesis. *Image and Vision Computing*, 149:105171, 2024.

Yonatan Geifman and Ran El-Yaniv. Selective classification for deep neural networks. *NeurIPS*, 2017.

Yonatan Geifman and Ran El-Yaniv. Selectivenet: A deep neural network with an integrated reject option. In *ICML*, 2019.

Yonatan Geifman, Guy Uziel, and Ran El-Yaniv. Bias-reduced uncertainty estimation for deep neural classifiers. In *ICLR*, 2019.

Robert Geirhos, Priyank Jaini, Austin Stone, Sourabh Medapati, Xi Yi, George Toderici, Abhijit Ogale, and Jonathon Shlens. Towards flexible perception with visual memory. *arXiv preprint arXiv:2408.08172*, 2024.

Dhruba Ghosh, Hannaneh Hajishirzi, and Ludwig Schmidt. Geneval: An object-focused framework for evaluating text-to-image alignment. *NeurIPS*, 2023.

Jianyang Gu, Samuel Stevens, Elizabeth G Campolongo, Matthew J Thompson, Net Zhang, Jiaman Wu, Andrei Kopanev, Zheda Mai, Alexander E White, James Balhoff, et al. Bioclip 2: Emergent properties from scaling hierarchical contrastive learning. *arXiv preprint arXiv:2505.23883*, 2025.

Chuan Guo, Geoff Pleiss, Yu Sun, and Kilian Q Weinberger. On calibration of modern neural networks. In *ICML*, 2017.

Ruiqi Guo, Philip Sun, Erik Lindgren, Quan Geng, David Simcha, Felix Chern, and Sanjiv Kumar. Accelerating large-scale inference with anisotropic vector quantization. In *ICML*, 2020.

Jack Hessel, Ari Holtzman, Maxwell Forbes, Ronan Le Bras, and Yejin Choi. Clipscore: A reference-free evaluation metric for image captioning. *arXiv preprint arXiv:2104.08718*, 2021.

Cheng-Yu Hsieh, Jieyu Zhang, Zixian Ma, Aniruddha Kembhavi, and Ranjay Krishna. Sugarcrape: Fixing hackable benchmarks for vision-language compositionality. In *NeurIPS*, volume 36, 2024.

Gabriel Ilharco, Mitchell Wortsman, Ross Wightman, Cade Gordon, Nicholas Carlini, Rohan Taori, Achal Dave, Vaishaal Shankar, Hongseok Namkoong, John Miller, Hannaneh Hajishirzi, Ali Farhadi, and Ludwig Schmidt. Openclip, July 2021. URL <https://doi.org/10.5281/zenodo.5143773>.

Jeremy Irvin, Pranav Rajpurkar, Michael Ko, Yifan Yu, Silviana Ciurea-Ilcus, Chris Chute, Henrik Marklund, Behzad Haghgoo, Robyn Ball, Katie Shpanskaya, et al. Chexpert: A large chest radiograph dataset with uncertainty labels and expert comparison. In *Proceedings of the AAAI conference on artificial intelligence*, volume 33, pp. 590–597, 2019.

Ahmet Iscen, Mathilde Caron, Alireza Fathi, and Cordelia Schmid. Retrieval-enhanced contrastive vision-text models. *arXiv preprint arXiv:2306.07196*, 2023a.

Ahmet Iscen, Alireza Fathi, and Cordelia Schmid. Improving image recognition by retrieving from web-scale image-text data. In *CVPR*, 2023b.

Alistair EW Johnson, Tom J Pollard, Seth J Berkowitz, Nathaniel R Greenbaum, Matthew P Lun-gren, Chih-ying Deng, Roger G Mark, and Steven Horng. Mimic-cxr, a de-identified publicly available database of chest radiographs with free-text reports. *Scientific data*, 6(1):317, 2019.

Amita Kamath, Jack Hessel, and Kai-Wei Chang. What’s “up” with vision-language models? investigating their struggle with spatial reasoning. *arXiv preprint arXiv:2310.19785*, 2023.

Patrick Lewis, Ethan Perez, Aleksandra Piktus, Fabio Petroni, Vladimir Karpukhin, Naman Goyal, Heinrich Kütller, Mike Lewis, Wen-tau Yih, Tim Rocktäschel, et al. Retrieval-augmented generation for knowledge-intensive nlp tasks. *Advances in neural information processing systems*, 33: 9459–9474, 2020.

Junnan Li, Dongxu Li, Caiming Xiong, and Steven Hoi. Blip: Bootstrapping language-image pre-training for unified vision-language understanding and generation. In *ICML*, 2022.

Tsung-Yi Lin, Michael Maire, Serge Belongie, James Hays, Pietro Perona, Deva Ramanan, Piotr Dollár, and C Lawrence Zitnick. Microsoft coco: Common objects in context. In *ECCV*, 2014.

Zhiqiu Lin, Deepak Pathak, Baiqi Li, Jiayao Li, Xide Xia, Graham Neubig, Pengchuan Zhang, and Deva Ramanan. Evaluating text-to-visual generation with image-to-text generation. In *European Conference on Computer Vision*, pp. 366–384. Springer, 2024.

Haotian Liu, Chunyuan Li, Qingyang Wu, and Yong Jae Lee. Visual instruction tuning. *NeurIPS*, 2023a.

Haotian Liu, Kilho Son, Jianwei Yang, Ce Liu, Jianfeng Gao, Yong Jae Lee, and Chunyuan Li. Learning customized visual models with retrieval-augmented knowledge. *arXiv:2301.07094*, 2023b.

Zixian Ma, Jerry Hong, Mustafa Omer Gul, Mona Gandhi, Irena Gao, and Ranjay Krishna. Crepe: Can vision-language foundation models reason compositionally? In *CVPR*, 2023.

George A Miller. Wordnet: a lexical database for english. *Communications of the ACM*, 38(11): 39–41, 1995.

Kengo Nakata, Youyang Ng, Daisuke Miyashita, Asuka Maki, Yu-Chieh Lin, and Jun Deguchi. Revisiting a knn-based image classification system with high-capacity storage. In *ECCV*, 2022.

Maria-Elena Nilsback and Andrew Zisserman. 102 category flower dataset. *Department of Engineering Science, University of Oxford. Retrieved March*, 4:2024, 2008.

Vicente Ordonez, Girish Kulkarni, and Tamara Berg. Im2text: Describing images using 1 million captioned photographs. *NurIPS*, 2011.

Adam Paszke, Sam Gross, Francisco Massa, Adam Lerer, James Bradbury, Gregory Chanan, Trevor Killeen, Zeming Lin, Natalia Gimelshein, Luca Antiga, Alban Desmaison, Andreas Kopf, Edward Yang, Zachary DeVito, Martin Raison, Alykhan Tejani, Sasank Chilamkurthy, Benoit Steiner, Lu Fang, Junjie Bai, and Soumith Chintala. Pytorch: An imperative style, high-performance deep learning library. In *NeurIPS*, 2019.

Bryan A Plummer, Liwei Wang, Chris M Cervantes, Juan C Caicedo, Julia Hockenmaier, and Svetlana Lazebnik. Flickr30k entities: Collecting region-to-phrase correspondences for richer image-to-sentence models. In *Proceedings of the IEEE international conference on computer vision*, pp. 2641–2649, 2015.

Alec Radford, Jong Wook Kim, Chris Hallacy, Aditya Ramesh, Gabriel Goh, Sandhini Agarwal, Girish Sastry, Amanda Askell, Pamela Mishkin, Jack Clark, Gretchen Krueger, and Ilya Sutskever. Learning transferable visual models from natural language supervision. In *ICML*, 2021.

Johannes Rückert, Louise Bloch, Raphael Brüngel, Ahmad Idrissi-Yaghir, Henning Schäfer, Cynthia S Schmidt, Sven Koitka, Obioma Pelka, Asma Ben Abacha, Alba G. Seco de Herrera, et al. Rocov2: Radiology objects in context version 2, an updated multimodal image dataset. *Scientific Data*, 11(1):688, 2024.

Ravi Shekhar, Sandro Pezzelle, Yauhen Klimovich, Aurelie Herbelot, Moin Nabi, Enver Sangineto, and Raffaella Bernardi. “foil it! find one mismatch between image and language caption”. In *Proceedings of the 55th Annual Meeting of the Association for Computational Linguistics (ACL) (Volume 1: Long Papers)*, pp. 255–265, 2017.

Junaid Shuja, Eisa Alanazi, Waleed Alasmary, and Abdulaziz Alashaikh. Covid-19 datasets: a survey and future challenges. *MedRxiv*, pp. 2020–05, 2020.

Thalles Silva, Helio Pedrini, and Adín Ramírez Rivera. Learning from memory: Non-parametric memory augmented self-supervised learning of visual features. *ICML*, 2024.

Khurram Soomro, Amir Roshan Zamir, and Mubarak Shah. Ucf101: A dataset of 101 human actions classes from videos in the wild. *arXiv preprint arXiv:1212.0402*, 2012.

Tejas Srinivasan, Jack Hessel, Tanmay Gupta, Bill Yuchen Lin, Yejin Choi, Jesse Thomason, and Khyathi Raghavi Chandu. Selective” selective prediction”: Reducing unnecessary abstention in vision-language reasoning. *arXiv preprint arXiv:2402.15610*, 2024.

Samuel Stevens, Jiaman Wu, Matthew J Thompson, Elizabeth G Campolongo, Chan Hee Song, David Edward Carlyn, Li Dong, Wasila M Dahdul, Charles Stewart, Tanya Berger-Wolf, Wei-Lun Chao, and Yu Su. Bioclip: A vision foundation model for the tree of life. In *CVPR*, 2024.

Tristan Thrush, Ryan Jiang, Max Bartolo, Amanpreet Singh, Adina Williams, Douwe Kiela, and Candace Ross. Winoground: Probing vision and language models for visio-linguistic compositionality. In *CVPR*, 2022.

Jeremias Traub, Till J Bungert, Carsten T Lüth, Michael Baumgartner, Klaus H Maier-Hein, Lena Maier-Hein, and Paul F Jäger. Overcoming common flaws in the evaluation of selective classification systems. *NeurIPS*, 2024.

Ramakrishna Vedantam, C Lawrence Zitnick, and Devi Parikh. Cider: Consensus-based image description evaluation. In *CVPR*, 2015.

Hualiang Wang, Yi Li, Huifeng Yao, and Xiaomeng Li. Clipn for zero-shot ood detection: Teaching clip to say no. In *ICCV*, 2023.

Lijie Wang, Xuetong Wang, Toshihiko Yamasaki, and Kiyoharu Aizawa. Aspect-ratio-preserving multi-patch image aesthetics score prediction. In *CVPRW*, 2019.

Liyuan Wang, Xingxing Zhang, Hang Su, and Jun Zhu. A comprehensive survey of continual learning: theory, method and application. *IEEE Transactions on Pattern Analysis and Machine Intelligence (TPAMI)*, 2024.

Pei Wang and Nuno Vasconcelos. Towards realistic predictors. In *ECCV*, 2018.

Spencer Whitehead, Suzanne Petryk, Vedaad Shakib, Joseph Gonzalez, Trevor Darrell, Anna Rohrbach, and Marcus Rohrbach. Reliable visual question answering: Abstain rather than answer incorrectly. In *ECCV*, 2022.

Tz-Ying Wu, Pedro Morgado, Pei Wang, Chih-Hui Ho, and Nuno Vasconcelos. Solving long-tailed recognition with deep realistic taxonomic classifier. In *ECCV*, 2020.

Chen-Wei Xie, Siyang Sun, Xiong Xiong, Yun Zheng, Deli Zhao, and Jingren Zhou. Ra-clip: Retrieval augmented contrastive language-image pre-training. In *CVPR*, 2023.

Michal Yarom, Yonatan Bitton, Soravit Changpinyo, Roei Aharoni, Jonathan Herzig, Oran Lang, Eran Ofek, and Idan Szpektor. What you see is what you read? improving text-image alignment evaluation. *Advances in Neural Information Processing Systems*, 36:1601–1619, 2023.

Ziyi Ye, Xiangsheng Li, Qiuchi Li, Qingyao Ai, Yujia Zhou, Wei Shen, Dong Yan, and Yiqun Liu. Learning llm-as-a-judge for preference alignment. In *ICLR*, 2025.

Zequan Zeng, Yan Xie, Hao Zhang, Chiyu Chen, Bo Chen, and Zhengjue Wang. Meacap: Memory-augmented zero-shot image captioning. In *CVPR*, 2024.

Xiaohua Zhai, Basil Mustafa, Alexander Kolesnikov, and Lucas Beyer. Sigmoid loss for language image pre-training. In *ICCV*, 2023.

Sheng Zhang, Yanbo Xu, Naoto Usuyama, Hanwen Xu, Jaspreet Bagga, Robert Tinn, Sam Preston, Rajesh Rao, Mu Wei, Naveen Valluri, et al. Biomedclip: a multimodal biomedical foundation model pretrained from fifteen million scientific image-text pairs. *arXiv preprint arXiv:2303.00915*, 2023.

Tiancheng Zhao, Tianqi Zhang, Mingwei Zhu, Haozhan Shen, Kyusong Lee, Xiaopeng Lu, and Jianwei Yin. Vi-checklist: Evaluating pre-trained vision-language models with objects, attributes and relations. *arXiv preprint arXiv:2207.00221*, 2022.

Kaiyang Zhou, Jingkang Yang, Chen Change Loy, and Ziwei Liu. Conditional prompt learning for vision-language models. In *CVPR*, 2022a.

Kaiyang Zhou, Jingkang Yang, Chen Change Loy, and Ziwei Liu. Learning to prompt for vision-language models. *International Journal of Computer Vision (IJCV)*, 130(9):2337–2348, 2022b.

Jinguo Zhu, Weiyun Wang, Zhe Chen, Zhaoyang Liu, Shenglong Ye, Lixin Gu, Hao Tian, Yuchen Duan, Weijie Su, Jie Shao, et al. Internvl3: Exploring advanced training and test-time recipes for open-source multimodal models. *arXiv preprint arXiv:2504.10479*, 2025.

The appendix is structured as follows -

1. Additional Implementation Details
 - Evaluation sets
 - Implementation
 - Algorithm
2. Comparison with baselines
 - PAPSP with SP-VLMs
 - Selective Predictors
 - Image-text alignment modules
 - LVLM-as-a-judge
 - SP-VLM Finetuning
 - Per-sample Inference Latency
3. Ablations
 - Neighborhood size
 - Size of Retrieval Set
 - Retrieval variants
 - Effect of relevance threshold
 - Contrastive component (CC)
4. More related works
 - Foundation Models for Scoring
5. Qualitative results

A ADDITIONAL IMPLEMENTATION DETAILS

In this section, we discuss additional implementation details of PAPSP and MA-PAPSP.

Evaluation Sets. Performance is evaluated on the test splits of the following datasets.

- *Selective classification*: Oxford Pets, Oxford Flowers (Nilsback & Zisserman, 2008) and UCF-101 (Soomro et al., 2012).
- *Selective image-text matching*. SugarCrepe (Hsieh et al., 2024), WinoGround (Thrush et al., 2022), What’sUp (Kamath et al., 2023), VL-Checklist (Zhao et al., 2022) and Foil (Shekhar et al., 2017).
- *Selective captioning*: MS-COCO (Lin et al., 2014) and Flickr-30K (Plummer et al., 2015).

Implementation. All experiments implemented using PyTorch (Paszke et al., 2019) and run on a single NVIDIA RTX 3090 GPU, using the pre-trained VLMs trained by OpenCLIP (Ilharco et al., 2021). The source codes of MA-PAPSP and PAPSP will be released upon publication.

Algorithm. The algorithm of MA-PAPSP is summarized in Algorithm A.1.

Algorithm A.1 MA-PAPSP

- 1: **Input:** image-caption pair $\mathbf{z} = \{\mathbf{v}, \mathbf{w}\}$, retrieval set $\mathcal{R} = \{\mathbf{x}_i, \mathbf{y}_i\}_{i=1}^N$
- 2: **Output:** score s
- 3: Compute $\mathcal{N}(\mathbf{v})$ using equation 5.
- 4: Compute proxy embedding $\tilde{\mathbf{w}}(\mathbf{v})$ using equation 6
- 5: **if** negative captions are present **then**
- 6: Compute s using equation 7
- 7: **else**
- 8: Generate \mathcal{E} for $f(\mathbf{x})$ using LLM
- 9: Compute s using equation 7
- 10: **end if**
- 11: return s

B COMPARISON WITH BASELINES

In this section, we compare MA-PAPSP to several baselines, including implementations of PAPSP with different SP-VLMs (OpenCLIP (Radford et al., 2021), EVA02 (Fang et al., 2024), SigLIP (Zhai et al., 2023)), other image-text alignment modules (GenEval (Ghosh et al., 2023), Aesthetics score (Wang et al., 2019)), retrieval-augmented CLIP (REACT (Liu et al., 2023b)), and finetuned SP-VLMs (SigLIP_{B/16}, SigLIP_{SO-400M}). Beyond this, we also consider models designed for selective

Model	MA	Classification			Captioning				ITM					
		Flowers	Pets	UCF101	MS-COCO Cider-N	Flickr-30K Meteor	Cider-N	Meteor	SugarCrepe	WinoGround	What'sUp	VL-Check	Foil	
Small Models														
OpenCLIP _{B/16}	✓	0.160 0.111	0.231 0.137	0.213 0.133	0.153 0.130	0.320 0.316	0.241 0.238	0.316 0.313	0.173 0.123	0.322 0.248	0.292 0.267	0.266 0.249	0.257 0.242	
EVA02 _{B/16}	✓	0.109 0.109	0.220 0.135	0.206 0.127	0.139 0.132	0.318 0.318	0.240 0.235	0.317 0.312	0.171 0.108	0.264 0.236	0.272 0.264	0.262 0.233	0.251 0.238	
SigLIP _{B/16}	✓	0.093 0.077	0.211 0.171	0.154 0.116	0.142 0.121	0.317 0.312	0.237 0.235	0.311 0.310	0.162 0.079	0.258 0.228	0.262 0.214	0.258 0.210	0.245 0.213	
Large Models														
OpenCLIP _{L/14}	✓	0.119 0.109	0.182 0.128	0.151 0.141	0.146 0.138	0.318 0.297	0.240 0.235	0.312 0.298	0.149 0.127	0.258 0.208	0.266 0.226	0.254 0.217	0.246 0.198	
EVA02 _{L/14}	✓	0.102	0.175	0.126	0.134	0.313	0.237	0.313	0.128	0.242	0.248	0.232	0.229	
SigLIP _{SO-400M}	✓	0.074 0.063	0.169 0.114	0.113 0.088	0.136 0.109	0.311 0.286	0.229 0.219	0.307 0.297	0.078 0.062	0.208 0.196	0.202 0.192	0.204 0.192	0.197 0.189	

Table A.1: AURC (↓) performance of PAPSP with and without memory augmentation (MA) for different visual language representation models.

prediction (LYP (Dancette et al., 2023), ReCoVERR (Srinivasan et al., 2024)), and LVLM-as-a-judge (Qwen-2.5-VL). Additionally, we analyze the inference latency of all methods. All experiments were conducted using the setup described in the main paper.

PAPSP with SP-VLMs. Table A.1 compares MA-PAPSP to PAPSP for different SP-VLMs, for all three tasks described in the main paper. The table supports the following conclusions. First, MA-PAPSP outperforms PAPSP consistently across tasks and datasets for both small and large SP-VLMs. Second, the gains of MA-PAPSP are larger for the larger SP-VLMs. This suggests that there is no saturation, *i.e.* even the largest VLRMs can benefit from the increase in representation stability and calibration afforded by MA-PAPSP.

Methods	Classification			Captioning				ITM				
	Flowers	Pets	UCF101	MS-COCO Cider-N	Flickr-30K Meteor	Cider-N	Meteor	SugarCrepe	WinoGround	What'sUp	VL-Checklist	Foil
LYP	0.216	0.221	0.226	0.152	0.342	<u>0.236</u>	0.323	<u>0.158</u>	0.229	<u>0.228</u>	<u>0.232</u>	0.225
ReCoVERR	0.225	0.216	0.223	0.142	0.336	<u>0.253</u>	0.327	0.167	<u>0.252</u>	<u>0.249</u>	<u>0.247</u>	0.242
PAPSP-S	0.093	0.211	0.154	0.142	0.317	0.237	0.311	0.162	0.258	0.262	0.258	0.245
MA-PAPSP-S	0.077	0.171	0.116	0.121	0.312	0.235	0.310	0.079	0.228	0.214	0.210	0.213
PAPSP-L	0.074	0.169	0.113	0.136	0.311	0.229	0.307	0.078	0.208	0.202	0.204	0.197
MA-PAPSP-L	0.063	0.114	0.088	0.109	0.286	0.219	0.297	0.062	0.196	0.192	0.192	0.189

Table B.1: AURC (↓) performance of PAPSP and MA-PAPSP to selective predictors.

Selective Predictors. Table B.1 compares MA-PAPSP to methods designed specifically for selective prediction (SP): LYP (Dancette et al., 2023) and ReCoVERR (Srinivasan et al., 2024). Phi-3.5-Instruct (3B) is used as the ReCoVERR LLM, and BLIP-2 is used as P-VLM for all methods. Shown in boldface are the overall best results, while the underlined results indicate where SP methods outperform PAPSP-S. PAPSP-L, and MA-PAPSP with both small and large model outperform both SP methods on 12/12 datasets. The gains are largest for MA-PAPSP-L. For instance, MA-PAPSP with small model has an AURC gain of 21 points and 18 Cider-N points over ReCoVERR on MS-COCO and Flickr-30K, respectively, while for MA-PAPSP with the largest model the gains become of 33 and 34 points, respectively. Note that this happens despite the fact that the SP models are computationally more intensive than MA-PAPSP and PAPSP.

Image-Text Alignment Modules. Table B.2 compares the performance of PAPSP and MA-PAPSP against state-of-the-art image-text alignment (ITA) models, including GenEval Score (Ghosh et al., 2023), Aesthetics Score (Wang et al., 2019), VQAScore (Lin et al., 2024) and SeeTRUE (Yarom et al., 2023). Boldface highlights the best-performing models, while the

Methods	Classification			Captioning				ITM							
	Flowers Pets UCF101			MS-COCO		Flickr-30K		SugarCrepe			Winoground		What'sUp	VL-Checklist	Foil
	Cider-N	Meteor	Cider-N	Meteor	Cider-N	Meteor	Cider-N	Sugar	Crepe	Winoground	What'sUp	VL-Checklist	Foil		
GenEval	0.216	0.213	0.226	0.155	0.327	0.249	0.317	0.149	0.246	0.240	0.234	0.217			
Aesthetics	0.212	0.211	0.225	0.155	0.322	0.242	0.318	0.153	0.241	0.241	0.227	0.221			
VQA-Score	0.211	0.207	0.217	0.146	0.321	0.241	0.312	0.146	0.240	0.236	0.226	0.217			
SeeTRUE	0.214	0.213	0.171	0.158	0.316	0.251	0.411	0.153	0.242	0.236	0.234	0.223			
PAPSP-S	0.093	0.211	0.154	0.142	0.317	0.237	0.311	0.162	0.258	0.262	0.258	0.245			
MA-PAPSP-S	0.077	0.171	0.116	0.121	0.312	0.235	0.310	0.079	0.228	0.214	0.210	0.213			
PAPSP-L	0.074	0.169	0.113	0.136	0.311	0.229	0.307	0.078	0.208	0.202	0.204	0.197			
MA-PAPSP-L	0.063	0.114	0.088	0.109	0.286	0.219	0.297	0.062	0.196	0.192	0.192	0.189			

Table B.2: AURC (\downarrow) for all three tasks. The table shows the comparison between PAPSP, MA-PAPSP and Image-text alignment modules.

underlined results indicate where ITA methods outperform PAPSP-S. PAPSP-L and MA-PAPSP with both small and large model outperform both ITA methods on 12/12 datasets. The gains of the larger versions of MA-PAPSP over ITA baselines are also more pronounced than for smaller models. Specifically, MA-PAPSP with the largest model outperforms the GenEval score by 44 points on MS-COCO and 30 points on Flickr-30K, under the Cider-N setting. This gain holds despite the fact that the ITA methods are significantly more computationally expensive than PAPSP and MA-PAPSP, as they rely on either visual-question answering with large vision-language models (LVLMs) or object detection combined with large language models (LLMs) to identify the presence of objects mentioned in the prompt. This again highlights the effectiveness of MA-PAPSP.

LVLM-as-Judge	Captioning				Classification			ITM						
	MS-COCO		Flickr-30K		Flowers Pets UCF-101			SugarCrepe		Winoground		What'sUp	VL-checklist	Foil
	Cider-N	Meteor	Cider-N	Meteor	Cider-N	Meteor	Cider-N	Meteor	Cider-N	Meteor	Cider-N	Meteor	Cider-N	Meteor
LVLM-PAPSP														
Qwen-VL-7B	0.120	0.301	0.233	0.312	0.075	0.126	0.099	0.073	0.209	0.205	0.205	0.202		
Qwen-VL-72B	0.115	0.294	0.227	0.305	0.070	0.120	0.094	0.068	0.203	0.199	0.199	0.196		
MA-PAPSP														
SigLIP _{SO-400M}	0.109	0.286	0.219	0.297	0.063	0.114	0.088	0.062	0.196	0.192	0.192	0.189		

Table B.3: Performance of MA-PAPSP as compared to LVLM-as-a-judge baselines.

LVLM-as-a-judge. We implemented a version of LVLM-as-judge, referred to as LVLM-PAPSP, which is comparable to PAPSP and MA-PAPSP. In this setup, an LVLM is tasked with generating an alignment score between the query image and its corresponding caption. This score is subsequently thresholded to facilitate selective prediction. Table B.3 presents the results for both the smaller (7B parameters) and larger (72B parameters) LVLMs from the Qwen-2.5-VL family. MA-PAPSP outperforms LVLM-PAPSP across all datasets and tasks, for both the 7B and 72B parameter models. These findings confirm the hypothesis that LVLMs are not well-calibrated to produce reliable confidence scores for selective prediction.

Model	Captioning				Classification			ITM						
	MS-COCO		Flickr-30K		Flowers Pets UCF-101			SugarCrepe		Winoground		What'sUp	VL-checklist	Foil
	Cider-N	Meteor	Cider-N	Meteor	Cider-N	Meteor	Cider-N	Meteor	Cider-N	Meteor	Cider-N	Meteor	Cider-N	Meteor
PAPSP	0.136	0.311	0.229	0.307	0.074	0.169	0.113	0.078	0.208	0.202	0.204	0.197		
PAPSP-FT	0.115	<u>0.278</u>	<u>0.224</u>	<u>0.301</u>	0.067	<u>0.074</u>	0.071	0.074	0.192	<u>0.188</u>	<u>0.202</u>	0.159		
MA-PAPSP	0.126	0.288	0.229	0.307	0.062	0.076	0.078	0.066	0.192	0.189	0.207	0.167		
MA-PAPSP-FT	0.104	0.234	0.217	0.288	0.060	0.068	0.072	0.064	0.188	0.172	0.201	0.162		

Table B.4: Performance of MA-PAPSP as compared to PAPSP and PAPSP with finetuned SigLIP_{SO-400M}. MA-PAPSP is implemented with SigLIP_{SO-400M}.

SP-VLM Finetuning. We evaluated the benefits of fine-tuning the SP-VLM on the in-domain dataset for both PAPSP and MA-PAPSP. In all experiments, the SP-VLM used was SigLIP_{SO-400M}, and the retrieval set for MA-PAPSP consisted of the in-domain dataset. The results are summarized

in Table B.4, were boldface denotes the best results and underline indicates when PAPSP-FT outperforms MA-PAPSP without finetuning. A few conclusions are possible. First, while PAPSP-FT outperforms MA-PAPSP on 9/12 datasets, the differences are small: around 10 points on MS-COCO, around 5 points on Flickr, between 2 and 7 points for the classification tasks, and between 1 and 8 points for ITM. Note that PAPSP-FT, requires training the SP-VLM for each retrieval set, which is cumbersome and computationally intensive. For example, finetuning the $\text{SigLIP}_{\text{SO-400M}}$ VLRM on the MS-COCO train split using a single RTX-A4000 requires 20 hours of training. The fact that MA-PAPSP is competitive *without any training* is a sign of its effectiveness. Second, if the training data available for finetuning is small, the finetuned VLRM can overfit leading to weak AURC. MA-PAPSP is more robust to small data sizes. For instance, in the ITM tasks, which tend to have small datasets (e.g. 1K samples for SugarCrepe), MA-PAPSP outperforms or is almost identical to PAPSP-FT on 3/5 datasets. Third, the best overall results are obtained with PAPSP-FT, which has the top performance in 10/12 datasets, and a loss of at most 3 points in the remaining 2/12. This shows that, even if a fine-tuned model is available (PAPSP-FT), MA-PAPSP is still beneficial. In fact the gains of MA-PAPSP-FT over PAPSP-FT can be larger than those of MA-PAPSP over PAPSP. For example, on Flickr-30K, MA-PAPSP has no gain over PAPSP but MA-PAPSP-FT has gains between 7 and 13 points over PAPSP-FT. In summary, the decision to finetune the SP-VLM must take into account whether the gains of PAPSP-FT over MA-PAPSP justify the additional training complexity. However, once the finetuned VLRM is available there is almost always a benefit in augmenting it with MA-PAPSP.

Methods	Time (ms) \downarrow
PAPSP-S/L	14.07/14.11
Close-set Task (Classification, ITM)	
MA-PAPSP-L (P)	14.87
Open-set Task (Captioning)	
MA-PAPSP-L (w RB) (P+C)	17.54
MA-PAPSP-L (w SLM) (P+C)	57.93
MA-PAPSP-L + PP (w SLM) (P+C)	25.85

Table B.5: Average inference times. P and C denote the two components of MA-PAPSP with RB or SLM, Proxy Embedding and Contrastive Score, respectively. PP denotes Pipeline parallelism over 2 GPUs.

Per-sample Inference Latency. Table B.5 presents a comparison of the inference time per sample across various methods. The top third of the table shows the inference times for PAPSP using both the small and large SP-VLMs, revealing that model size has minimal impact on latency. The middle third of the table displays the MA-PAPSP inference times for tasks, such as classification and ITM, that only require the computation of the proxy embedding (P). For these tasks, MA-PAPSP is comparable to PAPSP. The bottom third of the table shows the times for tasks like captioning, which involve both the proxy embedding and the contrastive score (P+C). This section highlights that the most time-consuming operation is the computation of contrastive scores, primarily due to the use of the LLM for generating hard negatives.

For captioning, MA-PAPSP is approximately three times slower than PAPSP. However, we note that several optimizations could significantly improve its speed. For instance, by employing pipeline parallelism across two RTX-3090 GPUs to parallelize the LLM and MA-PAPSP computations (denoted as MA-PAPSP-L+PP in the table), the overall inference time for MA-PAPSP can be reduced by more than half. Additionally, the nearest neighbor operation involved in proxy computation could be substantially accelerated using techniques such as Faiss (Douze et al., 2024), ScaNN (Guo et al., 2020), or indexing structures from classical retrieval methods (Lewis et al., 2020; Iscen et al., 2023a; Xie et al., 2023). The contrastive score computations could also be sped up significantly by replacing the LLM with rule-based sentence manipulations, as seen in prior work (Wang et al., 2024; Shekhar et al., 2017). While this approach could lead to slight degradation in AURC performance, it remains an avenue for future investigation. It is important to note that the computation of the retrieval set embeddings is a one-time operation and is not included in the times reported above, consistent with standard retrieval methods. For reference, the per-sample embedding time (on RTX-3090) and storage for CLIP_{B/16} are 10.361 ms and 2.274 KB, respectively.

Methods	Captioning				Classification			ITM					
	MS-COCO		Flickr-30K		Flowers	Pets	UCF101	SugarCrepe	WinoGround	What'sUp	VL-Checklist	Foil	
AUGRC Metric (\downarrow)													
PAPSP-S	0.207	0.331	0.224	0.365	0.106	0.185	0.124	0.189	0.293	0.311	0.271	0.272	
MA-PAPSP-S	0.165	0.318	0.219	0.319	0.087	0.162	0.118	0.168	0.226	0.278	0.262	0.253	
PAPSP-L	0.127	0.291	0.235	0.210	0.206	0.178	0.082	0.148	0.218	0.263	0.245	0.258	
MA-PAPSP-L	0.119	0.266	0.221	0.184	0.166	0.148	0.058	0.102	0.196	0.198	0.202	0.194	
AURC Metric (\downarrow)													
PAPSP-S	0.093	0.211	0.154	0.142	0.317	0.237	0.311	0.162	0.258	0.262	0.258	0.245	
MA-PAPSP-S	0.077	0.171	0.116	0.121	0.312	0.235	0.310	0.079	0.228	0.214	0.210	0.213	
PAPSP-L	0.074	0.169	0.113	0.136	0.311	0.229	0.307	0.078	0.208	0.202	0.204	0.197	
MA-PAPSP-L	0.063	0.114	0.088	0.109	0.286	0.219	0.297	0.062	0.196	0.192	0.192	0.189	

Table B.6: Selective prediction results on AUGRC (\downarrow) for AURC (\downarrow) metrics. S denotes the use of a small SP-VLM (SigLIP_{B/16}), while L denotes the larger SigLIP_{SO-400M}. In both cases, MA-PAPSP is implemented with the **out-of-domain** retrieval dataset.

Methods	Flowers	Pets	UCF101
PAPSP (SigLIP _{B/16})	0.100	0.112	0.157
MA-PAPSP (SigLIP _{B/16})	0.067	0.108	0.112
PAPSP (SigLIP _{SO-400M})	0.088	0.112	0.130
MA-PAPSP (SigLIP _{SO-400M})	0.054	0.101	0.119

Table B.7: AURC (\downarrow) for OOD detection.

Different Metrics. In the main paper, all evaluations are based on AURC scores. Recent work in selective prediction (Traub et al., 2024) has introduced alternative evaluation metrics. Table B.6 compares MA-PAPSP and PAPSP using the Area Under the Generalized Risk Coverage (AUGRC). While the absolute values differ, both metrics lead to the same conclusions.

Out-of-distribution detection. For classification tasks, selective prediction is usually important to distinguish out-of-distribution (OOD) samples from in-distribution (ID) samples. To evaluate MA-PAPSP in this setting, we considered the test splits of Oxford Pets, Oxford Flowers and UCF-101. In all cases, 80% of the classes were considered ID while the remaining 20% were considered OOD, and a classifier implemented for the ID classes. The largest class probability was used to implement selective prediction. Table B.7 summarizes the performance of PAPSP and MA-PAPSP for different SP-VLMs. For both small and large SP-VLMs, MA-PAPSP outperforms PAPSP in all datasets. In fact, MA-PAPSP with the small SP-VLM outperforms PAPSP with the large SP-VLM in all cases.

C ABLATIONS

This section contains more ablation results for MA-PAPSP.

Neighborhood size. The performance of MA-PAPSP depends on the neighborhood size K of (5), i.e. the size of set of texts retrieved from \mathcal{R} . Table C.1 shows an ablation for this parameter, for the captioning, image-text matching and classification tasks. Initially, as K increases, the AURC decreases, indicating better performance for larger retrieval sets. Note, in particular the advantages of the soft nearest neighbor embedding implemented by proxy embeddings over a hard nearest neighbor embedding, where just the top nearest neighbor is retrieved from \mathcal{R} . This corresponds to using $K = 1$. For all tasks and datasets, the soft nearest neighbor operation has better performance. These results confirm the importance of proxy embeddings that fuse information from several image-text pairs relevant to the query. However, beyond a certain K , performance starts to degrade, with AURC rising. This is because larger retrieval sets start to include irrelevant or poor matches, and the retrieved proxy is less related to the query. Such behavior is fairly common for nearest neighbor approaches. For both tasks, the best AURC score is achieved in the neighborhood of $K = 15$,

K	Captioning				Classification			ITM				
	MS-COCO		Flickr-30K		Flowers	Pets	UCF-101	SugarCrepe	Winoground	What'sUp	VL-checklist	Foil
Cider-N	Meteor	Cider-N	Meteor									
1	0.153	0.332	0.296	0.335	0.114	0.132	0.096	0.073	0.204	0.216	0.215	0.209
5	0.130	0.312	0.237	0.317	0.063	0.114	0.088	0.068	0.197	0.197	0.208	0.206
15	0.109	0.286	0.219	0.297	0.065	0.114	0.089	0.062	0.196	0.192	0.192	0.189
20	0.111	0.287	0.221	0.305	0.064	0.114	0.088	0.064	0.196	0.192	0.195	0.192

Table C.1: Neighborhood size K for all tasks.

\mathcal{R} Size/%	Captioning				Classification			ITM				
	MS-COCO		Flickr-30K		Flowers	Pets	UCF-101	SugarCrepe	Winoground	What'sUp	VL-checklist	Foil
Cider-N	Meteor	Cider-N	Meteor									
20	0.138	0.314	0.231	0.321	0.063	0.114	0.088	0.074	0.209	0.265	0.256	0.248
40	0.122	0.310	0.226	0.323	0.063	0.114	0.088	0.074	0.196	0.192	0.192	0.189
60	0.116	0.292	0.221	0.312	0.063	0.114	0.088	0.072	0.204	0.192	0.192	0.189
80	0.111	0.289	0.220	0.312	0.063	0.114	0.088	0.064	0.196	0.192	0.194	0.192
100	0.109	0.286	0.219	0.297	0.063	0.114	0.088	0.062	0.196	0.192	0.192	0.189

Table C.2: Performance of MA-PAPSP (SigLIP_{SO-400M}) versus the percentage of the retrieval dataset \mathcal{R} for all tasks. Retrieval set \mathcal{R} is in-domain.

suggesting an optimal balance between retrieval size and performance. We use this value as the default for MA-PAPSP in all experiments.

Size of Retrieval Set. To analyze the effect of size of retrieval set on the performance of MA-PAPSP, we randomly sub-sampled the *in-domain retrieval set*. Table C.2 shows that, as dataset size decreases, the performance of MA-PAPSP can degrade for the captioning task. This is because the samples relevant (nearest neighbors) to the query are removed from the retrieval set. However, for classification and ITM, performance stays mostly unaltered for sizes as low as 40%. This shows that these tasks are much less sensitive to the dataset size.

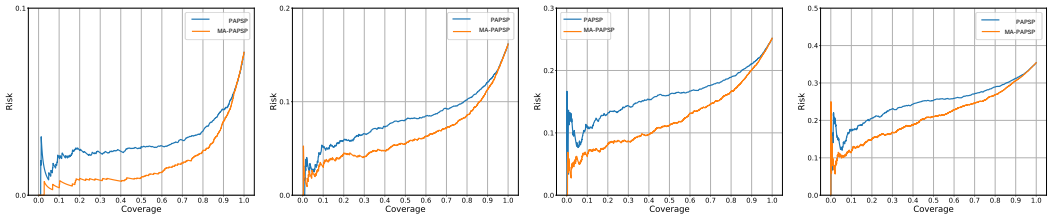
Retrieval variants. Experiments were performed to compare the performance of the different retrieval variants of Table 1, on the captioning, image-text matching and classification task, using a neighborhood size $K = 15$ and contrastive scoring. Table C.3 shows that, for the above tasks, image to text retrieval (i2tr) achieves the best performance under all metrics. This is consistent with previous observations that the CLIP similarity score (cosine similarity in CLIP embedding space) is more reliable when its two arguments are text embeddings, suggesting a better conceptual organization of the CLIP embedding for text (Iscen et al., 2023b). Since, under i2tr, the retrieved proxy is a proxy caption, i2tr is expected to outperform i2ir, which returns an image proxy. On the other hand, the use of the predicted caption $f(\mathbf{x})$ as a query is expected not to perform well, since any captioning errors will induce the retrieval of image-caption pairs from \mathcal{R} that are not relevant to the captioning of \mathbf{x} . This is true for other two tasks as well. It explains why the t2ir and t2tr variants do not perform well. Given these results, we use i2tr as the default retrieval implementation of MA-PAPSP. This variant is used in all other experiments of the paper.

Effect of relevance threshold. The evaluation of selective prediction requires the specification of threshold β in (3) for the risk computation. We ablated the importance of this threshold by plotting risk-coverage curves for different values of β . Figure C.1 shows an example for the Cider-N metric, for selective image captioning on the MS-COCO dataset, using MA-PAPSP and the OpenAI CLIP SP-VLM. While the four plots obtained with different values of β are different, the relative behavior of PAPSP and MA-PAPSP curves is similar, with MA-PAPSP achieving substantially lower risk for most coverage values. This shows that the exact value of β is not critical. Note, however, that the same threshold should be used across experiments that involve comparison of AURC curves. We have followed this practice in all experiments.

Contrastive component (CC). For tasks like image-text matching and classification, negative samples are available by definition of the task. For image captioning, we compare two alternatives for generating contrastive examples: a *rule-based* approach and an *LM-based* approach. The rule-based method involves substituting objects, attributes, or verbs in the caption using a predefined

Variant	Captioning				Classification				ITM				
	MS-COCO		Flickr-30K		Flowers	Pets	UCF-101		SugarCrepe	Winoground	What'sUp	VL-checklist	Foil
Cider-N	Meteor	Cider-N	Meteor										
i2ir	0.135	0.358	0.309	0.335	0.128	0.154	0.209		0.142	0.256	0.279	0.245	0.214
t2ir	0.152	0.344	0.264	0.342	0.116	0.118	0.164		0.116	0.242	0.266	0.242	0.208
t2tr	0.162	0.367	0.269	0.341	0.106	0.126	0.169		0.128	0.238	0.257	0.231	0.216
i2tr	0.109	0.286	0.219	0.297	0.063	0.114	0.088		0.062	0.196	0.192	0.192	0.189

Table C.3: Retrieval Variants for all tasks.

Figure C.1: Risk-Coverage curves of CLIP and PAPSP for selective image captioning under the Cider-N ($N = 4$) metric, for different values of the threshold β used to define the risk. Left to right: $\beta = 0.2$, $\beta = 0.4$, $\beta = 0.6$, $\beta = 0.8$.

Variant	MS-COCO		Flickr-30K		Inference Time
	Cider-N	Meteor	Cider-N	Meteor	
MA-PAPSP without CC					
MA-PAPSP	0.143	0.323	0.239	0.316	-
MA-PAPSP w/ Rule-based CC					
Rule-Based	0.113	0.301	0.222	0.301	4.72 ms
MA-PAPSP w/ LLM-based CC - Small LLM					
Qwen-2.5 _{3B}	0.117	0.306	0.213	0.304	42.26 ms
Phi-3.5 _{3B}	0.109	0.286	0.219	0.297	41.06 ms
MA-PAPSP w/ LLM-based CC - Large LLM					
Qwen-2.5 _{7B}	0.111	0.283	0.217	0.278	84.96 ms
Llama-3 _{8B}	0.108	0.277	0.219	0.276	92.65 ms

Table C.4: Selective captioning AURC (↓) for different methods of contrastive component (CC).

set of rules. We used SpaCy to identify the part of speech—such as noun, adjective, or verb—and then replaced the identified word with another one from WordNet (Miller, 1995). In contrast, the LM-based method takes a given context (provided in E) and prompt and outputs a modified prompt with swapped objects, attributes, and verbs. Unlike the rule-based approach, the LM-generated captions are generally more coherent and grammatically correct as shown in E a. Table C.4 shows that, in addition to faster inference of the rule-based approach than that of LM-based methods, it is able to perform at par with even the implementation of MA-PAPSP with a LLM. For example MA-PAPSP with Phi-3.5 has just an improvement of 4 points over MA-PAPSP with rule based contrastive scores for MS-COCO with Cider-N setting. This indicates more effective generation of contrastive samples. Further, while larger LLMs achieve better results, the differences are not very significant. For example, Llama-3 (8B parameter model) has an improvement of 1 point over Phi-3.5 (3B) for MS-COCO (Cider-N), but its inference time is almost double (92.65ms vs 43.06ms of Phi-3). Due to its better trade-off between performance and computation overhead, we use the rule-based approach in all our experiments.

D MORE RELATED WORKS

In this section, we talk about using more works that are related to MA-PAPSP.

Foundation Models for Scoring. Visual language representation models, like CLIP (Radford et al., 2021), extract features from vision-language pairs and use contrastive learning (Ding et al., 2021) to learn a space where the two modalities are aligned. This enables the design of alignment scores based on simple operations, like cosine similarity, that underlie measures like the CLIP score (Hessel et al., 2021). Thresholding the CLIP score is a low-complexity solution for selective prediction, which we denote as PAPSP and use as baseline. MA-PAPSP improves on this baseline.

E QUALITATIVE RESULTS

We have presented the following two sets of qualitative figures - first, to show how the proxy component helps MA-PAPSP perform better than the baseline CLIP scores, we visualize some retrieved samples in Figures E.3, E.4, E.5 and E.6. Next, figure E.1 shows the prompt we were using to generate contrastive.

You are an intelligent and helpful AI assistant that can do the following task. Given an input context describing a scene, your task is to identify all the noun phrases in the sentence and then create a new sentence from all those noun phrases. The new sentence must meet the following four requirements:

1. The new sentence must be fluent and grammatically correct.
2. The new sentence must make logical sense.
3. The new sentence must not add any new noun phrases, but it must have all the noun phrases of the original sentence.

Here is one example:

Example 1: Sentence - A man and a woman are walking together.
New sentence: A man and a woman are talking to each other."
Explanation: There are two noun phrases in the sentence - man and woman. So, the new sentence contains those two noun phrases. It is different from the given context and does not include any extra noun phrases.

Generate 3 new sentences for this prompt. Do NOT give any explanation
Context - <prompt>
System:

Figure E.1: LLM Prompt used to generate negatives from a given prompt.

Examples of negative captions:

Main caption – A desk with a computer, a monitor, and a phone.
RB approach – A room with a man, a dog, and a airplane.
LM approach – A table with a glass of water and a fishbowl.

Main caption – A woman sitting on a bench on a city street.
RB approach – A boat sitting on a school on a rainbow.
LM approach – A man sitting on a chair in a quiet room.

Figure E.2: Example of negative captions generated by LM and RB.

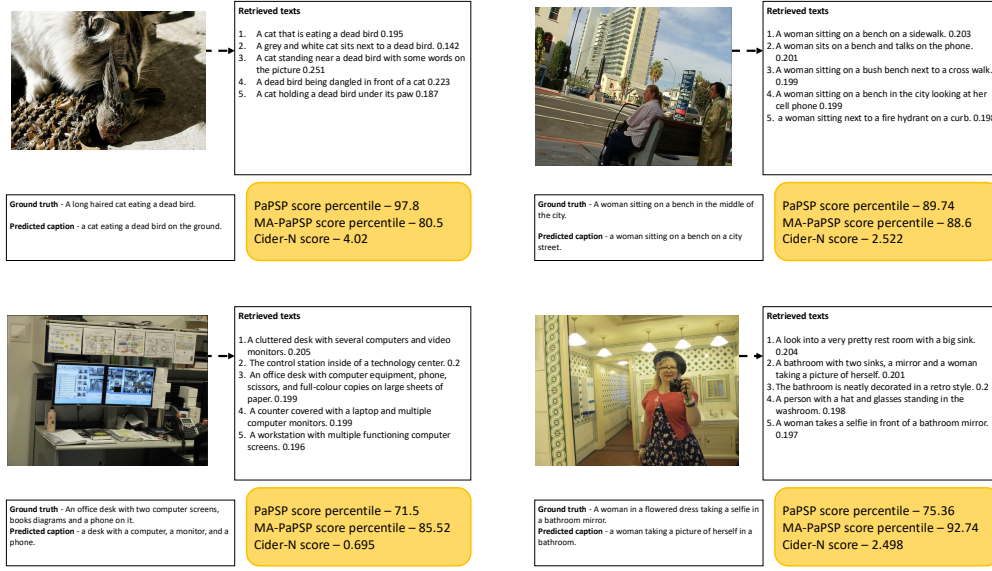


Figure E.3: This figure presents examples where both PAPSP and MA-PAPSP accept the inputs. Each example includes the following components: the image, its predicted caption, the ground-truth caption, the retrieved captions along with their normalized weights, PAPSP baseline scores, MA-PAPSP scores, and the ground-truth score (Cider-N).

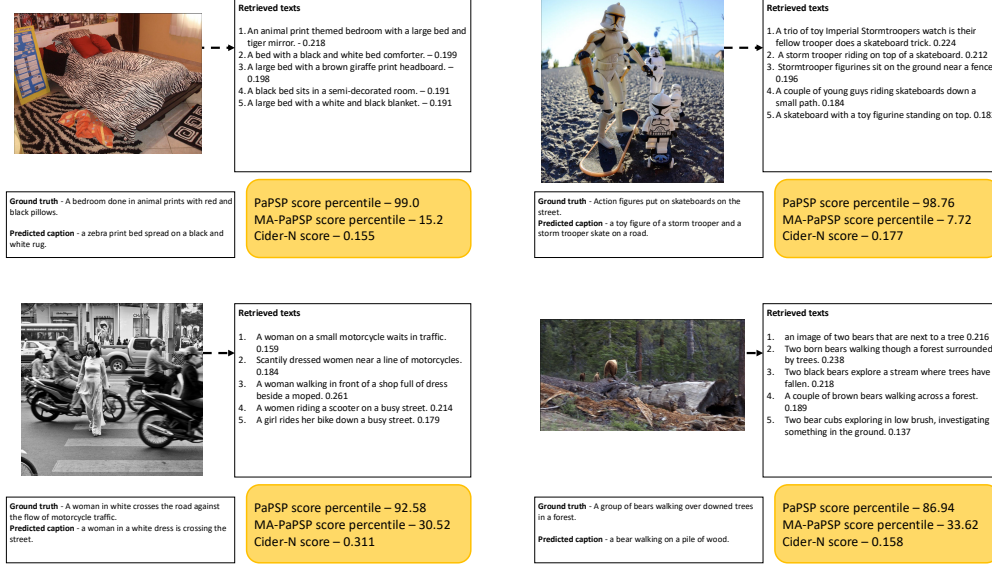


Figure E.4: This figure presents examples where PAPSP accepts and MA-PAPSP rejects the inputs. Each example includes the following components: the image, its predicted caption, the ground-truth caption, the retrieved captions along with their normalized weights, PAPSP baseline scores, MA-PAPSP scores, and the ground-truth score (Cider-N).

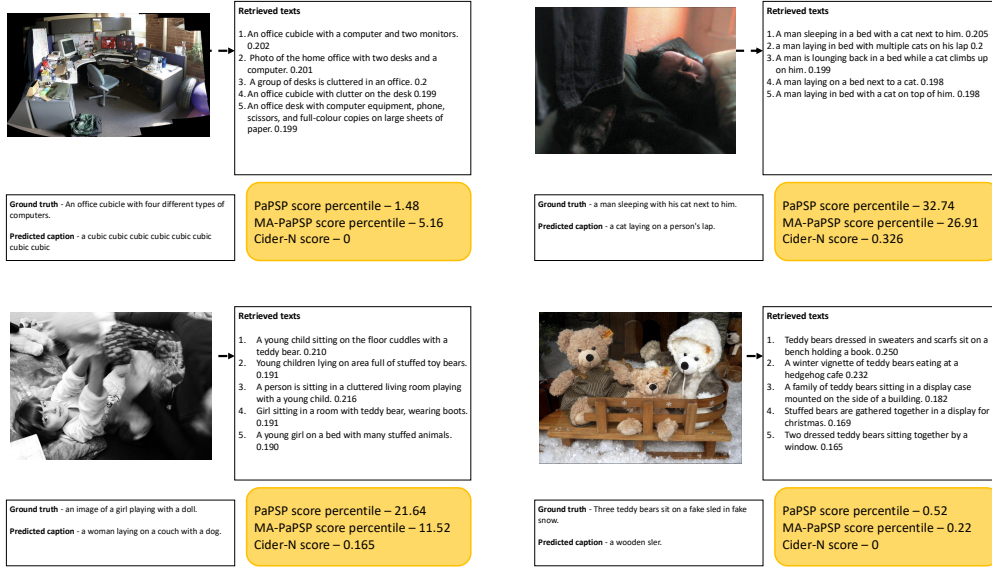


Figure E.5: This figure presents examples where both PAPSP and MA-PAPSP reject the inputs. Each example includes the following components: the image, its predicted caption, the ground-truth caption, the retrieved captions along with their normalized weights, PAPSP baseline scores, MA-PAPSP scores, and the ground-truth score (Cider-N).

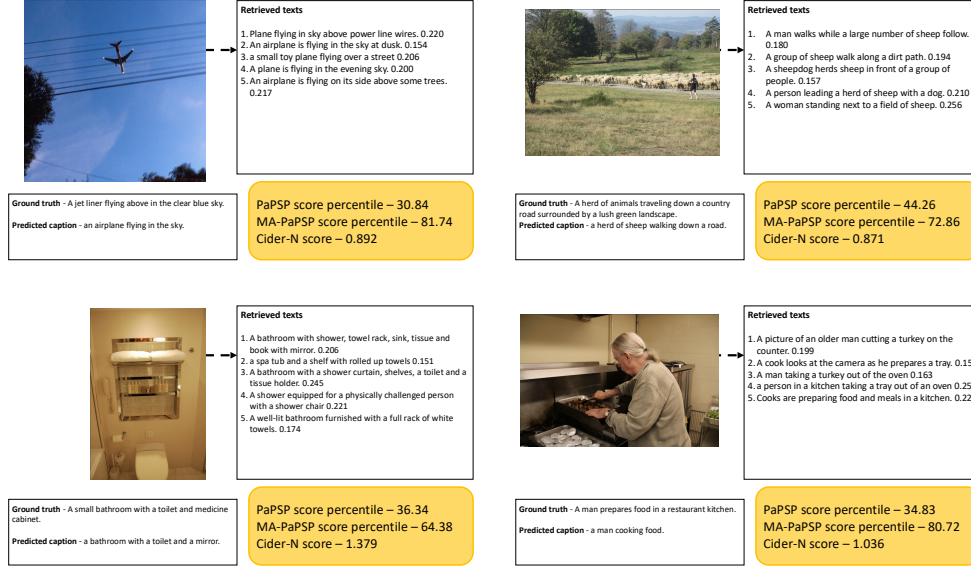


Figure E.6: This figure presents examples where PAPSP rejects and MA-PAPSP accepts the inputs. Each example includes the following components: the image, its predicted caption, the ground-truth caption, the retrieved captions along with their normalized weights, PAPSP baseline scores, MA-PAPSP scores, and the ground-truth score (Cider-N).